JANA MÜNCHENBERGER

MEMRISTIVE SYSTEMS AND THEIR APPLICATIONS

BIELEFELD UNIVERSITY

Memristive systems and their applications

By Jana Münchenberger

Declaration:
The work in this thesis is my own original work, none but the indicated resources were used.

Copyright © 2012 Jana Münchenberger
Bielefeld University
Department of Physics
Thin Films & Physics of Nanostructures

Reviewers:
PD Dr. A. Thomas,
Prof. Dr. Jürgen Schnack

The chapter *A memristor based on current induced domain* is based on the paper: J. Münchenberger, G. Reiss, and A. Thomas *A memristor based on current-induced domain-wall motion in a nanostructured giant magnetoresistance device*, Journal of Applied Physics **111**, 07D303 (2012)

The chapter *Resistive switching in memristive tunnel junctions and its application* is based on the paper: J. Münchenberger, P. Krzysteczko, G. Reiss, and A. Thomas, *Improved reliability of magnetic field programmable gate arrays through the use of memristive tunnel junctions*, Journal of Applied Physics, **110**, 096105–096105 (2011)

The section *Spike timing dependant plasticity in memristive MTJs* in chapter *Application of memristive MTJs in artificial neuronal systems* is based on the paper: P. Krzysteczko, J. Münchenberger, M. Schäfers, G. Reiss, and A. Thomas *The Memristive Magnetic Tunnel Junction as a Nanoscopic Synapse-Neuron System*, Advanced Materials, **24**, 762–766 (2012), Figure 3b.

Bielefeld, March 2012

Acknowledgments

I would like to thank my supervisors PD Dr. Andy Thomas and Prof. Dr. Günter Reiss for the opportunity to work in their research groups and their excellent advice during the creation of this thesis.

I sincerely thank Dr. Karsten Rott for help with all technical problems, in particular with the the e-beam lithography and the maintenance of various machines.

I would like to say thanks for helpful discussions with my colleagues and the pleasant work environment. Special thanks to Inga-Mareen Imort, Savio Fabretti and Nadine Mill as well as to my former colleague Dr. Patryk Krzysteczko who passed the memristive MTJs and the collaboration with Münster to me and was always open for helpful discussion.

Infineon Regensburg as well as Singulus are thankfully acknowledged for providing samples.

I thankfully acknowledge the collaboration with Dr. Vladislav Demidov and Prof. Dr. Sergej Demokritov from the university of Münster.

Contents

List of publications 7

Introduction 9

A memristor based on current induced domain wall motion 17

Resistive switching in memristive tunnel junctions and its application 29

Application of memristive MTJs in artificial neuronal systems 41

Conclusion 55

Appendix 57

List of publications

First author publications

J. Münchenberger, P. Krzysteczko, G. Reiss, and A. Thomas, *Improved reliability of magnetic field programmable gate arrays through the use of memristive tunnel junctions*, Journal of Applied Physics, **110**, 096105–096105 (2011)

J. Münchenberger, G. Reiss, and A. Thomas *A memristor based on current-induced domain-wall motion in a nanostructured giant magnetoresistance device*, Journal of Applied Physics **111**, 07D303 (2012)

Coauthor publications (Bielefeld)

V. Drewello, M. Schäfers, O. Schebaum, A. A. Khan, J. Münchenberger, J. Schmalhorst, G. Reiss, and A. Thomas, *Inelastic electron tunneling spectra of MgO-based magnetic tunnel junctions with different electrode designs*, Physical Review B **79**, 174417 (2009)

P. Krzysteczko, J. Münchenberger, M. Schäfers, G. Reiss, and A. Thomas *The Memristive Magnetic Tunnel Junction as a Nanoscopic Synapse-Neuron System*, Advanced Materials, **24**, 762–766 (2012)

Coauthor publications in cooperation with workgroup Demokritov (Münster)

V. E. Demidov, M. Buchmeier, K. Rott, P. Krzysteczko, J. Münchenberger, G. Reiss, and S. O. Demokritov, *Nonlinear Hybridization of the Fundamental Eigenmodes of Microscopic Ferromagnetic Ellipses*, Physical Review Letters **104**, 217203 (2010)

J. Jersch, V. E. Demidov, H. Fuchs, K. Rott, P. Krzysteczko, J.

Münchenberger, G. Reiss, and S. O. Demokritov, *Mapping of localized spin-wave excitations by near-field Brillouin light scattering*, Applied Physics Letters **97**, 152502 (2010)

V. E. Demidov, M. P. Kostylev, K. Rott, J. Münchenberger, G. Reiss, and S. O. Demokritov, *Excitation of short-wavelength spin waves in magnonic waveguides* , Applied Physics Letters **99**, 082507 (2011)

Conferences

DPG Frühjahrstagung 2010, Regensburg, Germany *Resistance tuning of GMR devices via domain wall motion* (poster)

DPG Frühjahrstagung 2011, Dresden, Germany *Controlling the resistance of a micro-/nanostructured GMR device with current induced domain wall motion* (poster)

MMM 2011, Scottsdale, Phoenix, AZ, USA, *Realization of a memristor by current induced domain wall motion in a micro-/nanostructured GMR device* (poster)

Introduction

After the proposal of the memristor in 1971 by Chua[1] and its realization in 2008 by HP researchers,[2] a search for new materials and devices to realize further memristive systems started. In this thesis those systems and their application are explored utilizing well known effects and technologies such as giant magnetoresistance and tunnel magnetoresistance.[3] [4]

The application of giant magnetoresistance devices and magnetic tunnel junctions has been widely established since the discovery of both effects. Both proved to be reliable building blocks in wide number of areas, such as sensors, read heads for hard disk drives, as well as components of magnetic random access memory and magnetic field programmable gate arrays.[5]

Introducing memristive behavior into such systems gives the opportunity to implement interesting new concepts into established technologies improving, for example their error tolerance. It also allows to include and explore new features such as neuronal behavior in such devices.

The understanding of the human brain still remains one of the final frontiers in science. While the newest technologies were always consulted in attempts to model it, true progress was only made with the evolution of computer technology and growing processing power. The field of computational neuroscience and neuro-informatics developed models to simulate artificial neural networks. This area of research has evolved so far that it is now reported to emulate the brain of rather far developed animals such as cats.[6] From this it is merely a matter of decades and growing computational power to simulate the brains of animals like primates and maybe even humans.[7] Despite the success to simulate brains and nerves with common technology, the idea to build electronic circuit elements that directly replicate the functionality of neurons, is intriguing. At this point the memristor has its appearance, since similar behavior is predicted in this device.

An outline of the thesis is given in the course of this introduc-

[1] L. O. Chua, IEEE Transactions on circuit theory **CT-18** (1971) 507–519

[2] D.B. Strukov et al., Nature **453** (2008) 30–83

[3] M. N. Baibich et al., Phys. Rev. Lett. **61** (1988) 2472–2475; G. Binasch et al., Phys. Rev. B **39** (1989) 4828–4830; P. Grünberg et al., Phys. Rev. Lett. **57** (1986) 2442–2445

[4] M. Julliere, Phys. Lett. **54 A** (1975) 225–226; T. Miyazaki and N. Tezuka, J. Magn. Magn. Mater. **139** (1995) L231 –L2340; J. S. Moodera et al., Phys. Rev. Lett. **74** (1995) 3273–3276

[5] D. Meyners et al., J. Appl. Phys. **99** 023907; G. A. Prinz, Science **282** (1998) 1660–1663; R. Richter et al., Appl. Phys. Lett. **80** (2002) 1291–1293; Jr. W. C. Black and B. Das, J. Appl. Phys. **87** (2000) 6674–6679

[6] R. Ananthanarayanan et al., in, Proceedings of the Conference on High Performance Computing Networking, Storage and Analysis, SC '09, Portland, Oregon: ACM, 2009, 63:1–63:12

[7] See: *The Human Brain Project*

tion. Prior to the outline however, it is necessary to make a short digression about the fourth circuit element, the memristor, since the term is used throughout the thesis.

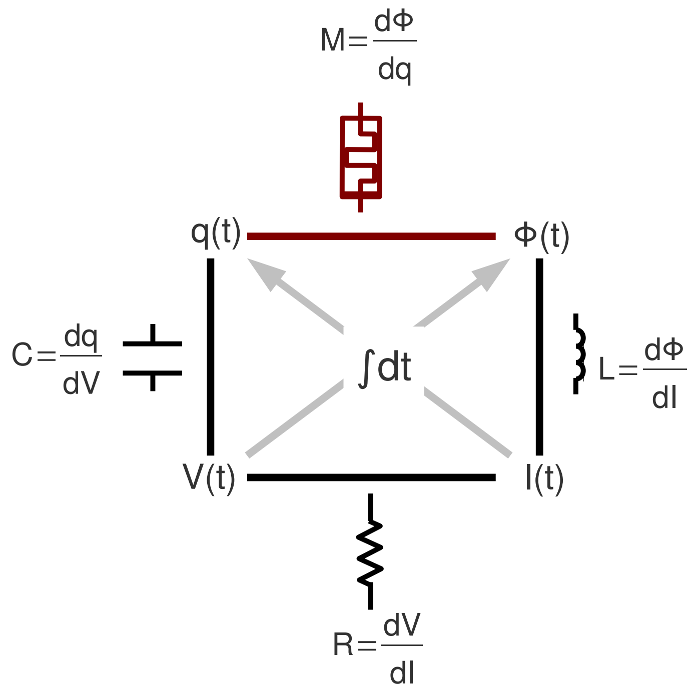

Figure 1: Chuas symmetry considerations. This sketch is based on said considerations and the sketch of D.B. Strukov et al., Nature **453** (2008) 30–83. The classic circuit elements capacitor, resistor and inductor are listed as well as their corresponding properties capacity C, resistance R and inductance L. The expressions relates these properties to the four fundamental variables V, I, q and Φ. Based on the symmetry there has to be a fourth circuit elements, relating Φ to q its missing property is called memristance M.

The Memristor

The most cited paper regarding the proposal of the memristor is *Memristor the missing circuit element* from L. Chua in 1971.[8] In Figure 1 a sketch of Chuas considerations is shown. The existence of the memristor is suggested based on theoretical symmetry considerations of classic circuit elements and on how the four fundamental variables, voltage $V(t)$, current $I(t)$, (magnetic) flux $\Phi(t)$ and electrical charge $q(t)$ are connected: Voltage and flux as well as current and charge are related over their time integrals.

[8] L. O. Chua, IEEE Transactions on circuit theory **CT-18** (1971) 507–519

The properties capacity C, resistance R and inductance L of the the classic circuit elements capacitor, resistor and inductor can be expressed as the differential relation of the four fundamental variables. The capacity C calculates from the relation between electric charge and voltage. The connection between voltage and current produces the resistance R, while the inductance L constitutes the relation between the current and the magnetic flux (see Figure 1).

Concluding from the sketch there now has to be a fourth fundamental circuit element based on a connection between flux and charge. The missing variable is called *memristance* M and the corresponding circuit element *memristor*.

The voltage across a charge controlled memristor is generally given by the expression:

$$V(t) = M(q(t))I(t) \tag{1}$$

with M as a function of q. Whereas the charge is expressed as the time integral over the current:

$$q(t) = \int_0^t I(t^*)dt^* \tag{2}$$

and the memristance M is given by

$$M(q) = \frac{d\Phi(q(t))}{dq}. \tag{3}$$

What can be concluded from these equations is that the state of the memristor is dependent on the history of the current $I(t)$ or the voltage $V(t)$, respectively. Hence, the name *Memristor* was established as a combination from the words *memory* and *resistor*. Rewriting equation 1 to:

$$M(q(t)) = \frac{V(t)}{I(t)}, \tag{4}$$

the name becomes clear, as the equation 4 closely resembles the normal resistance, save for the dependency of the current history. In 1976, the described concept was generalized to broader class of memristive systems.[9] Here a current controlled memristive device can be described with the equations:

[9] L. O. Chua and Sung Mo Kang, Proceedings of the IEEE **64** (1976) 209–223

$$V(t) = M(w, I(t))I(t)) \tag{5}$$

$$\frac{dw}{dt} = f(w, I(t)) \tag{6}$$

Here w is a set of state variables and M and f are in general explicit time dependent functions. The description above includes the pure memristor for $M(w, I(t)) = M(w)$ and $\frac{dw}{dt} = I(t)$, as well as the classic resistor for $M(w, I(t)) = M(w)$ and $\frac{dw}{dt} = 0$. Figure 2 shows a curve of a memristor. Typical for this devices is the hysteretic behavior that shows in the splitting at the end of the curves.

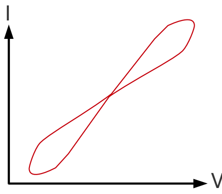

Figure 2: IV-curve of a memristive device with the characteristic splitting in the curve.

Before dealing with the realization of such a device some comments are necessary: Most realizations are more or less memristive systems instead of actual pure memristors; they are called memristors nonetheless. The term flux Φ refers to a general flux, not the magnetic flux exclusively. Most publications about memristors refer to the deduced definition in equation 4, rather than the flux definition. It can be reasoned that it is more vivid to imagine a resistor which state is based on the current history than to use the rather formal definition via the flux.

Realization and application of memristive systems

Ironically, the first realization of a memristive device took place eleven years before the actual proposal of the memristor in 1971 by Chua. It was developed by B. Widrow in 1960 and was called memistor by Widrow.[10] It was based on a pencil lead that was electroplated with copper. The rate of deposition, respectively resolution of the copper in an electrolytic bath was used to tune the resistance of the device. Widrow also pointed out the dependency of the devices resistance on the history of the plating current. While his results were purely means to the ends to create an artificial, adaptive neuron and lacked the systematic Chua developed eleven years later, they are impressive anyways. Building artificial neurons and neuronal nets from memristors has peaked interest ever since a memristor was realized by the HP researchers Strukov et al.[11] after over 30 years of stagnation in the field. This memristor is based on a Pt | TiO_2 | Pt sandwich that uses resistive switching to gain memristive behavior. Strukov's work led to new interest in the field. After this initial paper, various memristive systems were proposed and realized such as memristive magnetic tunnel junctions[12], systems based on current induced domain wall motion[13], nanoparticles[14] and even out of the ordinary ideas like human blood.[15]

[10] B. Widrow, Stanford Electronics Laboratories Technical Report **1553** (1960)

[11] D.B. Strukov et al., Nature **453** (2008) 30–83

[12] P. Krzysteczko, G. Reiss and A. Thomas, Appl. Phys. Lett. **95** 112508(2009) 112508; P. Krzysteczko et al., J. Magn. and Magn. Mater. **321** (2009) 144 –147

[13] J. Münchenberger, G. Reiss and A. Thomas, J. Appl. Phys. **111** (2012) 07D303; X. Wang et al., Electron Device Letters, IEEE **30** (2009) 294 –297

[14] T. H. Kim et al., Nano Lett. **9** (2009) 2229–2233

[15] S. P. Kosta et al., International Journal of Medical Engineering and Informatics **3** (2011) 16 –29

Being able to build memristive systems, the question remains how these systems can be utilized. Like most new innovations in this area, application in data storage and processing come to

mind and were pointed out by Borghetti et al.[16] The hypothetical, continuously tunable resistance of a memristor could bring new impulses in those fields. The application of memristors in artificial neuronal systems and nets to imitate biological learning behavior was already thought of by Widrow in 1960 and again proposed almost immediately after the publication of Strukov's discovery in 2008. In the last three years, memristors were utilized to imitate the learning behavior of the amoeba *Physarum polycephalum* in reaction to heating and cooling, as well as for pattern recognition in more complex systems.[17] [18] Another branch of research deals with modeling basic synaptic and neuronal behavior to comprehend and copy the functionality of the nervous system and brain on a basic level.[19]

[16] J. Borghetti et al., Nature **464** (2010) 873–876

[17] Y. V. Pershin, S. La Fontaine and M. Di Ventra, Phys. Rev. E **80** (2009) 021926

[18] G. S. Snider, Nanotech. **18** (2007) 365202

[19] K. Seo et al., Nanotech. **22** (2011) 254023

Outline of the thesis

The thesis at hand consists of three main building blocks as pictured in Figure 3. These building blocks are arranged to present the development of a memristive system, the classic application and further characterization of an already developed memristive system and at last the application of the same system in artificial neuronal systems. Each chapter features a short introduction into the topic as well as the analysis of the obtained data. It closes with a discussion of the results and a short conclusion. Below a short abstract for each chapter is given. The chapters are thematically based on three papers: [20] [21] [22]

[20] J. Münchenberger, G. Reiss and A. Thomas, J. Appl. Phys. **111** (2012) 07D303

[21] J. Münchenberger et al., J. Appl. Phys. **110** (2011) 096105 –096105

[22] P. Krzysteczko et al., Adv. Mater. (2012) 762–766

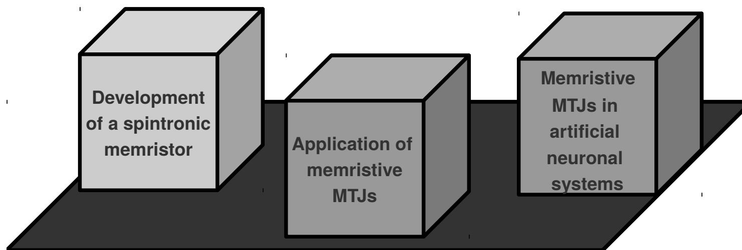

Figure 3: Outline of the thesis

A memristor based on current induced domain wall motion

The possibility of controlling the resistance of a memristive giant magnetoresistance[23] -system via current-induced domain-wall motion is investigated. A transition from multi domain states to single domain states takes place, if the lateral size of a magnetic layer is constricted. Current-induced domain-wall motion is predicted for such a narrow structure, as soon as the current density reaches a critical threshold.[24] The spin-polarized current exerts a torque on the domain wall, moving it through the structure. The investigated GMR-systems exhibit two resistance-states, depending on their magnetic orientation. Those states are referred to as high-resistance-state (HRS) and low-resistance-state (LRS). Current-induced domain-wall motion in the free layer can be detected for a narrow spin-valve structure, once the current density exceeds a critical threshold. In this case, the resistance of the device depends on the position of the domain wall. This behavior corresponds to a linear memristor.[25]

A giant magnetoresistance system is structured by e-beam lithography and ion beam etching to realize this device. With a constant current source, measurements are performed to determine the critical current density both with and without applying an external assisting magnetic field. Micromagnetic simulations allow to estimate the domain wall velocity as well as the time scale necessary for the operation of the device. Basic pulse measurements are conducted to show, that it is possible to adjust the resistance of this memristor in small steps.

[23] M. N. Baibich et al., Phys. Rev. Lett. **61** (1988) 2472–2475; G. Binasch et al., Phys. Rev. B **39** (1989) 4828–4830; P. Grünberg et al., Phys. Rev. Lett. **57** (1986) 2442–2445

[24] L. Berger, J. Appl. Phys. **55(6)** (1984) 1954–1956; J. C. Slonczewski, J. Magn. Magn. Mater. **159** (1996) L1 –L7

[25] J. Münchenberger, G. Reiss and A. Thomas, J. Appl. Phys. **111** (2012) 07D303; X. Wang et al., Electron Device Letters, IEEE **30** (2009) 294 –297

Resistive switching in memristive magnetic tunnel junctions and its application

The successful implementation of the long-hypothesized memristor sparked increasing attention for its use in neuronal computing and in the reproduction of biological neural networks. The growing number of devices with memristive properties is promising to improve already established technologies, in addition to the development of these new applications.

Magnetic tunnel junctions are electronic devices characterized by two ferromagnetic electrodes separated by a tunnel barrier. They exhibit low- or high-resistance-states when the electrodes are in parallel or antiparallel orientations, respectively. This phenomenon is referred to as tunnel magnetoresistance.[26] This chapter investigates the dependency of the memristive effect[27] in magnesium-oxide-based magnetic tunnel junctions[28] on the

[26] M. Julliere, Phys. Lett. **54 A** (1975) 225–226

[27] P. Krzysteczko, G. Reiss and A. Thomas, Appl. Phys. Lett. **95** 112508(2009) 112508; P. Krzysteczko et al., J. Magn. and Magn. Mater. **321** (2009) 144 –147

[28] W. H. Butler et al., Phys. Rev. B **63** (2001) 054416; J. Mathon and A. Umerski, Phys. Rev. B **63** (2001) 220403; S. S. P. Parkin et al., Nature Mater. **3** (2004) 862 –867; S. Yuasa et al., Nature Mater. **3** (2004) 868 –871

amplitude of the applied stress voltage is determined while the time interval of the stress pulse is kept constant. Furthermore, the dependency on the duration of the stress pulse is measured for a constant amplitude of the applied stress voltage.

The application of the effect in magnetic random access memory and magnetic field programmable gate arrays[29] was hypothesized as well as implemented after the observance of tunnel magnetoresistance at room temperature.[30] However, it has been shown that fluctuations in the resistance of the junctions can severely limit their use in field programmable gate arrays. This chapter shows, how the memristive properties of the tunnel junctions can be used to improve the error tolerance of said devices by compensating for the resistance fluctuations.[31]

[29] G. A. Prinz, Science **282** (1998) 1660–1663; Jr. W. C. Black and B. Das, J. Appl. Phys. **87** (2000) 6674–6679

[30] T. Miyazaki and N. Tezuka, J. Magn. Magn. Mater. **139** (1995) L231 – L2340; J. S. Moodera et al., Phys. Rev. Lett. **74** (1995) 3273–3276

[31] J. Münchenberger et al., J. Appl. Phys. **110** (2011) 096105 –096105

Application of memristive magnetic tunnel junctions in artificial neuronal systems

Ever since their discovery, memristors are suggested to be used to simulate nerves and, ultimately, the brain due to their unique characteristics. Like in a system of nerve cells, their state is dependent on their history. Also, they adapt to stimuli, which is why the first (unwitting) prototype of the memristor in 1960 was build specifically to simulate a neuron.

This chapter shows, how memristive magnetic tunnel junctions are used to simulate the behavior of a biological synapse. In synapses adaptive behavior towards incoming stimuli (action potentials) can be observed. These stimuli can result in a weakening or a strengthening of the synaptic connection, called Long Term Depression (LTD) and Long Term Potentiation (LTP). Furthermore synapses are able to add up incoming stimuli with a certain temporal delay. This behavior is called Spike Timing Dependent Plasticity (STDP) and is rebuild in the memristive magnetic tunnel junctions.[32]

[32] P. Krzysteczko et al., Adv. Mater. (2012) 762–766

Anyway, a single synapse does not make a brain. Therefore, the second part of this chapter investigates and characterizes a system of two coupled memristors. As an outlook the idea is entertained to create an array of memristive synapses in combination with CMOS pre- and post-neurons.

A memristor based on current induced domain wall motion

Basic concept

Ferromagnetic materials in general and magnetic thin films in particular exhibit magnetic domains and, therefore, magnetic domain walls. If a magnetic thin film is constricted in a further dimension, a transition from multi domain to single-domain states can be observed.[33] These can be moved through the narrow stripe by either applying a magnetic field or a current as predicted by Berger in 1978:[34] A spin-polarized current can apply a torque to a magnetic domain wall. Current induced domain wall motion can be observed if the current density j exceeds a critical current density j_c.[35] A spin-polarized current arises if electrons move through ferromagnets. The scattering rate is higher for those electrons with a spin antiparallel to the ferromagnet's orientation. A good perspective of the topic is given by Beach et al.[36]

The described system of a single magnetic layer can be expanded to a giant magnetoresistance (GMR) system.[37] This consists of two ferromagnetic layers that are separated by a nonmagnetic layer. In Figure 4 such a system is shown. The lower ferromagnet is primed to have a higher coercive field than the upper ferromagnetic layer. This can either be accomplished by antiferromagnetic interlayer coupling or by choosing different materials or layer thicknesses. A third way is an (artificial) antiferromagnet that is used for the so-called pinning.[38] Here the additional antiferromagnet fixes the orientation of the bottom magnetic layer in one direction. The orientation of this layer is only reversible by a magnetic field significantly stronger than those necessary for switching the orientation of the top layer. This provides a stable configuration of two states where the magnetic layers are oriented either parallel or antiparallel in respect to each other. Only the top layer changes its orientation. Hence

[33] B. Hausmanns, Dissertation, Universität Essen/Duisburg, 2003

[34] L. Berger, J. Appl. Phys. **49** (1978) 2156 –2161

[35] L. Berger, Phys. Rev. B **54** (1996) 9353–9358; L. Berger, J. Appl. Phys. **55(6)** (1984) 1954–1956; J. C. Slonczewski, J. Magn. Magn. Mater. **159** (1996) L1 –L7

[36] G.S.D. Beach, M. Tsoi and J.L. Erskine, J. Magn. Magn. Mater. **320** (2008) 1272 –1281

[37] M. N. Baibich et al., Phys. Rev. Lett. **61** (1988) 2472–2475; G. Binasch et al., Phys. Rev. B **39** (1989) 4828–4830; P. Grünberg et al., Phys. Rev. Lett. **57** (1986) 2442–2445

[38] J. Nogués and I. K. Schuller, J. Magn. Magn. Mater. **192** (1999) 203 –232

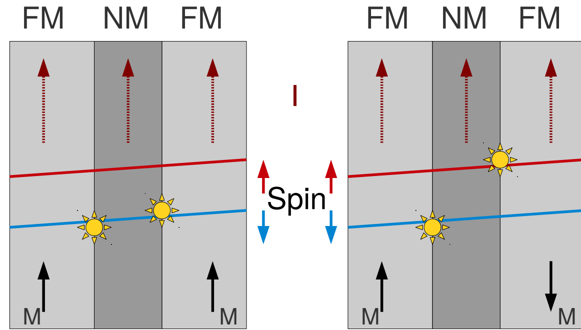

Figure 4: Mott-two-current-model of the GMR-effect as featured by Fert. In dependency of the magnetic orientation spin scattering takes place on the interfaces of the trilayer. If the spin-orientation is antiparallel to the orientation of the magnetization the electrons have a higher scattering rate. The scattering processes are indicated by the small suns. The dotted arrows show the current direction in CIP-geometry, while the lines indicate possible paths through the layers.

the upper layer is called *free layer* and the bottom layer *fixed layer*.

The GMR systems show a dependency of the resistance-states on the angle between the magnetization of the two ferromagnetic layers. A low resistance state (LRS) is exhibited for the parallel orientation of the layers, for the antiparallel orientation the system shows a high resistance state (HRS). Mott's two-current-model[39] provides an intuitive description of the change in the resistance depicted in Figure 4. It is presumed that the spin quantum number of conduction electrons is conserved during the vast majority of the scattering processes. This leads to the assumption that the total conductivity can be expressed by summing the contributions of the spin-up and spin-down electrons. If the system is measured in the current in plane (CIP)-geometry (in case of a parallel orientation of the magnetization) the GMR arises if the mean free path for one spin-direction is larger than the mean free path of the second spin direction. In the following, for simplicity only scattering on the interfaces is considered: The scattering is strong for electrons with a spin antiparallel and weak for spins parallel to the orientation of the magnetization (as can be seen in Figure 4). The ferromagnetic layers act as spin selective valve. The direction of magnetization determines which spin direction is more easily transmitted. The resistance through the system is low in the parallel orientation for one spin-direction, which

[39] N. F. Mott, Proc. R. Soc. Lond. **A 153** (1936) 699–717

leads to a low total resistance. Scattering takes place for both spin directions in the antiparallel orientation, which leads to a high total resistance.

If $R^{\uparrow}$ and $R^{\downarrow}$ are the resistances for spin-up and spin-down direction, the resistance in the parallel (p) and antiparallel (ap) case are given as:

$$R_p = (\frac{1}{R^{\uparrow}} + \frac{1}{R^{\downarrow}})^{-1} \tag{7}$$

and

$$R_{ap} = \frac{R^{\uparrow} + R^{\downarrow}}{4} \tag{8}$$

It is now possible to define a scattering asymmetry parameter $\alpha = \frac{R^{\uparrow}}{R^{\downarrow}}$. Accordingly, the GMR ratio can be calculated to:

$$GMR := \frac{(1-\alpha)^2}{4\alpha} = \frac{R_{ap} - R_p}{R_p} \tag{9}$$

For $R_{ap} \geq R_p$ this leads to a positive GMR. The details of transport phenomena and spin-dependent scattering processes in ferromagnets in such trilayers are described in detail by U. Hartmann et al.[40]

[40] U. Hartmann et al., Springer, 1999

Similar to the single magnetic layer a transition to single domain states occurs once a GMR-system is structured in a further dimension as depicted in Figure 5. If the critical current density j_c is reached it is possible to move the domain wall through the free layer.[41] The magnetization of the free layer in reference to the fixed layer is controlled by the position of the domain wall. Since the magnetization of the free layer controls the resistance of the stripe, it is possible to adjust the resistance of the stripe by the position of the domain wall:[42]

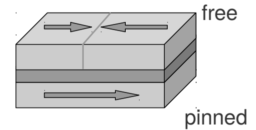

Figure 5: Memristor based on current induced domain wall motion in the free layer. The arrows indicate the magnetization of the layers. If the current density is higher than the critical current density, the domain wall can be moved through the stripe.

[41] J. Grollier et al., Appl. Phys. Lett. **83** (2003) 509–511

[42] Y. Chen and X. Wang, in, IEEE/ACM International Symposium on Nanoscale Architectures, 2009. NANOARCH '09., 2009, 7 –12; X. Wang et al., Electron Device Letters, IEEE **30** (2009) 294 –297

$$R = r_h \cdot x + r_l(D - x) \tag{10}$$

R is the resistance of the memristor, r_h and r_L are the resistances per unit length in the parallel and antiparallel case respectively, D is the length of the stripe and x the domain wall position. Therefore, it should be possible to move the domain wall continuously through the structure and get a linear progression of the resistance. The result would be a linear memristor. This device also has nonvolatile resistance-states as long as the current applied to read-out the memristors state is below the critical current.

The Landau-Lifshitz-Gilbert equation is used for a general theoretical description of such a dynamic magnetic system:[43]

[43] T. L. Gilbert, Physical Review **100** (1955) 1243; T.L. Gilbert, Magnetics, IEEE Transactions on **40** (2004) 3443 –3449; L. D. Landau and E. M. Lifshitz, Phys. Z. Sowjet. **8** (1935) 153 –169

$$\frac{\partial \vec{M}}{\partial t} = -\frac{\gamma}{1+\alpha^2}\vec{M}\times\vec{H}_{eff} - \frac{\gamma\alpha}{(1+\alpha^2)M_S}\vec{M}\times(\vec{M}\times H_{eff}) \quad (11)$$

Here $\vec{M}$ is the magnetization, α the Gilbert-damping parameter, $\vec{H}_{eff}$ the effective magnetic field, γ the gyro-magnetic ratio and M_S the saturation magnetization. Spin torque terms have to be added to include the current induced domain wall motion.[44] These consider the influence of a spin polarized current, which exerts a torque to the magnetization of a domain wall, leading to the motion of the domain wall. For a motion in x-direction along the wire the equation is given as:

[44] A. Thiaville et al., Europhys. Lett. **69** (2005) 990; A. Vanhaverbeke and M. Viret, Phys. Rev. B **75** (2007) 024411; S. Zhang and Z. Li, Phys. Rev. Lett. **93** (2004) 127204

$$\frac{\partial}{\partial t}\vec{m} = -|\gamma|\vec{H}_{eff}\times\vec{m}+\alpha\vec{m}\times\frac{\partial}{\partial t}\vec{m}+u\cdot\vec{m}\times(\vec{m}\times\frac{\partial\vec{m}}{\partial x})+\beta\cdot u\cdot\vec{m}\times\frac{\partial\vec{m}}{\partial x} \quad (12)$$

Here $\vec{m} = \frac{\vec{M}}{M_S}$ is the unit-vector of the magnetization, the dimensionless parameter β describes the nonadiabaticity of the system, while u is a velocity-equivalent, which reads:

$$u = \frac{jgP\mu_B}{2eM_S} \quad (13)$$

Here j is the current-density, g the Landé-factor, P the current polarization of the used material, μ_B the Bohr magnetron, e the elementary charge and M_S the saturation magnetization.

Methods and measurements

A GMR-system was provided by Infineon Regensburg for the preparation of the memristor. It has the following layer sequence: (bottom) Si | Ta 3 | Py 2 | PtMn 15 | CoFe 2 | Ru 1 | CoFe 2 | Cu 2 | CoFe 5 | TaN 10 (top). The layer thicknesses are given in nanometers. It was fabricated by sputter deposition.[45] The TaN acts as a capping layer. The bottom ferromagnetic layer is pinned by an artificial antiferromagnet. It has a high switching field of > 4500 Oe. The 5 nm thick CoFe layer is the active element of the memristor. The GMR of the system is about 10%, as prepared. The samples are structured in a two step lithography process by e-beam lithography and ion-beam-etching. First the stripes are written into negative e-beam resist. After the etching and the removal of the resist the structure is covered with 6 nm of Ta and 35 nm Au by sputter deposition. In the second step the contacts pads are structured by the same procedure. The details concerning the structuring can be found in the *Appendix*.

[45] A. Elshabini-Riad and F. D. Barlow III, McGraw Hill, 1998; J. A. Venables, Cambridge University Press, 2000; K. Wasa and S. Hayakawa, Noyes Publications, 1992

Figure 6 depicts a scanning electron microscopy (SEM)-images of the stripe: On the left, the image displays an overview of the stripe with a diamond-shaped domain wall nucleation pad and parts of the conductive paths to the contact pads. The right picture shows a close-up of the stripe. The stripes have a width of about 200 nm. The samples are glued to IC-packages with conductive silver for the measurement.

The measurements are conducted in CIP-geometry. The four-point-method with a constant current source at room temperature is used: A current is applied between the outer contacts, while the voltage is measured between the two inner contacts. To test the samples, a GMR-curve is measured by applying a constant current and varying the magnetic field. In Figure 7 a typical minor loop of a sample is depicted. The samples show a GMR ratio of about 8%. The diminished effect compared to the as-prepared case can be explained by defects and edge effects caused by the lithography. Furthermore, the GMR-curve shows a sharp switching behavior, without steps, which suggests only few pinning centers for the domain wall within the structure.

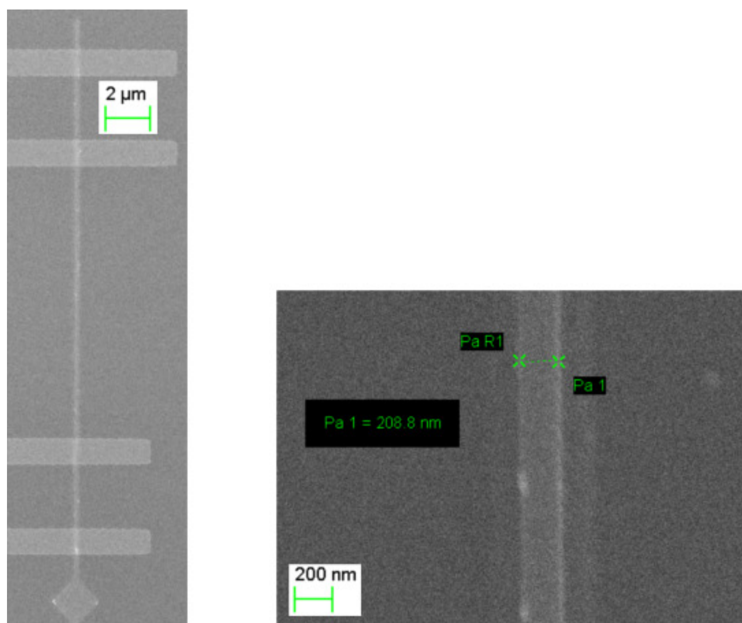

Figure 6: SEM-images of the memristor. The left image shows an overview over the structure with the domain wall nucleation pad and parts of the conductive paths to the contact pads. The current is applied between the outer conductive paths. The voltage is measured between the inner ones. The right image is a close up of the stripe.

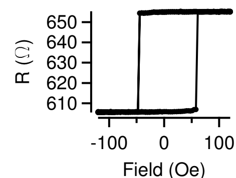

Figure 7: GMR-curve of a memristor based on current induced domain wall motion with an GMR-effect of about 8%.

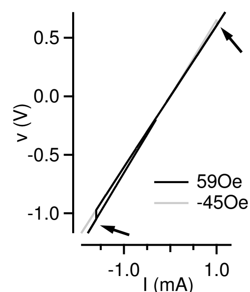

Figure 8: IV-curve of the stripe. The arrow indicate the splitting at the ends, that is characteristic for memristors.

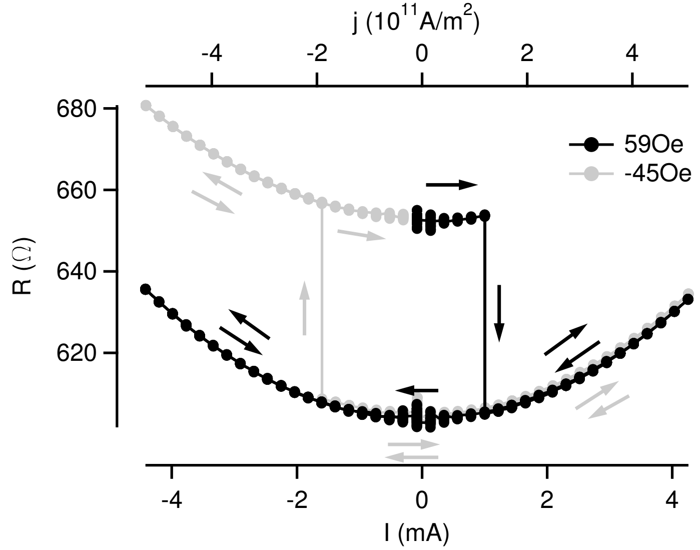

Figure 9: Resistance vs. current and current density measured at applied bias fields. The warping in the curve is due to Joule heating. The critical current densities are reached at $-1.9 \cdot 10^{11}$ A/m² for a bias field of −45 Oe and $1.2 \cdot 10^{11}$ A/m² for 59 Oe. The arrows indicate the course of the resistance for both field directions.

A magnetic field is applied prior to the measurement to induce a domain wall in the structure. Additionally, external magnetic fields −45 Oe and 59 Oe near the switching field of the GMR-curve are applied during the actual measurement to reduce the critical current density. Afterwards, an IV-curve is measured. From the IV-curve the resistance in dependency of the applied current can be determined. The measurement time of the constant-current-source is set to 500 ms to provide for a precise control of the current. Figure 8 depicts the IV-curve which shows a splitting at the ends that is characteristic for a memristive system.

In Figure 9 the resistance versus the applied current and current density is shown. The current density in the stripe calculates to:

$$j = \frac{I}{b \cdot h} \tag{14}$$

Here I is the applied current, $b = 200$ nm the width of the stripe and $h = 42$ nm the height of the layer stack. To allow the calculation of the current density it is assumed that the current flow is equal in all layers. Figure 9 shows two consecutive measurements. A distinct switching between resistance states is discernible at certain current densities. Also the resistance-states are stable until further interaction with the system. Further interaction means,

that again a current above the critical threshold is applied. The amplitude of the resistance change matches the amplitude of the field induced switching. Therefore there is a transition between parallel and antiparallel orientation of the magnetic layers. The effect amplitude (EA) calculates analog to the GMR ratio:

$$EA := \frac{R_{high} - R_{low}}{R_{low}} \quad (15)$$

The arrows in Figure 9 indicate the course of the resistance for both field directions. The distortion of the resistance curve aside from the sharp switching occurs due to Joule heating of the sample at high currents. The temperature difference between zero current and maximum current is calculated by the linear approximation:[46]

$$R_T = R_0[1 + \alpha(T - T_0)] \quad (16)$$

Here R_0 and R_T are the resistances at zero current and maximum current, T_0 the room temperature and T the temperature with Joule heating. α is the temperature coefficient of resistance that is material-specific. For metals it is in between $3 \cdot 10^{-3}$ and $6 \cdot 10^{-3}$. Considering the different metals in the GMR system the range of the Joule heating has to be estimated. Solving the equation for T, the temperature difference due to the heating is in between 10 K and 27 K. The critical current densities of $-1.9 \cdot 10^{11}$ A/m² and $1.2 \cdot 10^{11}$ A/m² match those of similar systems.[47]

[46] H. Kuchling, Fachbuchverlag Leipzig im Carl Hanser Verlag, 2011

[47] Y. Jang et al., Nanotech. **20** 125401

Simulation vs. measurement

While the overall change in the resistance can be measured, the conducted experiment does not allow to estimate the velocity of a domain wall moving through the stripe. Micromagnetic simulations are performed to obtain this information. The object oriented micromagnetic framework (OOMMF)-package[48] from the NIST was used for this purpose to simulate the system. An add-on for the OOMMF-package that takes the current induced domain wall motion into account was developed by IBM Zürich.

The program numerically solves the Landau-Lifshitz-Gilbert-equation with the spin torque term along the wire to calculate the domain wall motion. Only the motion of the domain wall in the 5 nm thick CoFe free layer is considered in the simulation of the investigated system. The add-on of IBM Zürich was originally designed to simulate a transverse domain wall in permalloy. Given the thickness of the free layer the domain wall in the experimental stack is likely a transverse domain wall.[49] The material-

[48] M.J. Donahue and D.G. Porter, Interagency Report **NISTIR 6376** (1999) National Institute of Standards and Technology, Gaithersburg, MD, URL: `http://math.nist.gov/oommf`

[49] G.S.D. Beach, M. Tsoi and J.L. Erskine, J. Magn. Magn. Mater. **320** (2008) 1272–1281

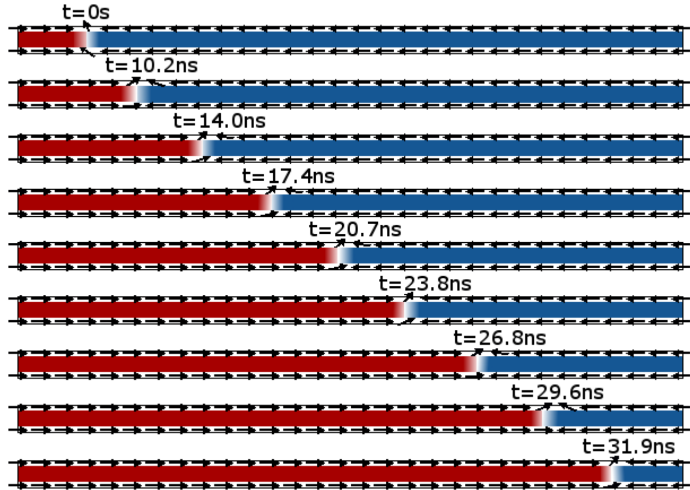

Figure 10: Simulated motion of the domain wall along the wire at zero field and a current density of $5.6 \cdot 10^{11}$ A/m². The magnetization of the stripe is displayed by arrows and color.

specific values like the saturation magnetization are adjusted from permalloy to those of CoFe.

An external magnetic field of 50 Oe is applied for the first simulations. The size of the simulated stripe is 5 nm×200 nm×5 µm. A saturation magnetization of $1300 \cdot 10^3$ A/m as well as a current polarization of 0.8 are assumed for CoFe.[50] For the critical current density the measured value of $1.2 \cdot 10^{11}$ A/m² is employed. The velocity equivalent then calculates to $u = 3.5$ m/s (cp. equation 13). The domain wall is fixed at one end of the stripe at the beginning of the simulation. As an additional parameter the exchange constant is set to $A = 3 \cdot 10^{12}$ J/m, the Gilbert damping constant is set to $\alpha = 0.005$ and the non-adiabaticity parameter is set to $\beta = 0.04$. The simulation results show a velocity of 100 m/s for the domain wall.

[50] P. M. Braganca et al., Nanotech. **21** (2010) 235202; Y. Ren et al., Appl. Phys. Lett. **92** (2008) 162513

Simulations at zero magnetic field were performed to verify the calculations, determining the critical current density necessary for domain wall motion, which can be measured. Figure 10 shows the motion of the domain wall through the stripe at zero magnetic field. The different magnetization directions are color-coded. The simulated current density is $5.6 \cdot 10^{11}$ A/m², which corresponds to a velocity equivalent of $u = 20$ m/s. The velocity of the domain wall calculates to 125 m/s. An actual measurement on a structured GMR system at zero field exhibits a switching

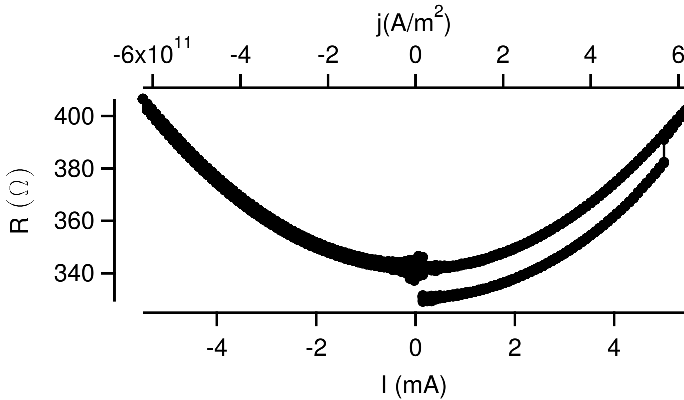

Figure 11: Measured switching curve of a memristor at zero field at a current density of $5.72 \cdot 10^{11}$ A/m². The two different resistance states were used to calculate the steps in Figure 12.

at around $5.72 \cdot 10^{11}$ A/m² (see: Figure 11). This matches the simulated value considering that a real wire likely features imperfections, that act as pinning centers for domain walls due to the lithography process. Figure 12 presents the course of the resistance and the domain wall displacement depending on the time for the simulated stripe. The resistance change is approximately linear after a phase of acceleration of the domain wall. For the calculation of the resistance change, the resistance of the sample in Figure 11 was used.

It was shown that it is possible to build a linear memristor based on current induced domain wall motion in a structured

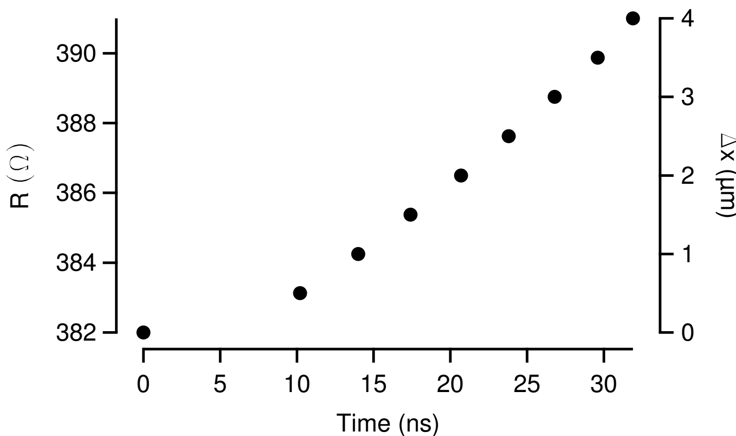

Figure 12: Simulated course of the resistance and domain wall displacement as function of time. After an acceleration time of about 10 ns the motion of the domain wall can be assumed as linear ($v = const.$) reasonably well.

GMR system. This prototype can be switched between its resistance states even without an applied external magnetic field. The splitting in the IV-curve shows a general memristive characteristic. Simulations were performed to determine the time scale of the domain wall motion. To control the domain wall position on a length scale of 0.5 µm the time resolution has to be below 4 ns for the zero field measurements. Recent publications show detailed control over domain walls using pulses of nanosecond length to check the domain wall position.[51] The application of short pulse techniques thus would allow tuning the resistance between the resistance states. This behavior corresponds to a linear memristor since the direction of the resistance change depends reproducibly on the current pulse direction.

[51] L. Heyne et al., Appl. Phys. Lett. **96** (2010) 032504; X. Jiang et al., Nano Lett. **11** (2011) 96–100

Pulse measurements

While the equipment to measure domain wall motion on the time scale with precisely formed pulses it not at hand in Bielefeld at the moment, it is possible to do basic pulse measurements with a existing constant current source despite its slow control rate. The constant current source is not able to provide pulses with a defined form for high currents (high means above the critical threshold) or a pulse length below 100 ms. Nevertheless, pulses with a form resembling the one depicted in Figure 13 can be created. The pulse length can be modified until a pulse with a wide base is generated which possesses a narrow peak that is near or just above the critical current. While the exact pulse-form stays undefined, the amplitude of the pulse can be controlled.

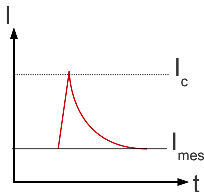

Figure 13: Pulse from the constant current source. The pulse has a narrow peak just above the critical current density j_c and a wide base.

A structured stripe is stressed with a series of alternating read and write pulses. The current of the read pulses is below the critical threshold. Another layout was used for the measurement. It has the domain wall nucleation pad in the middle of the structure and the stripe itself is longer. The changed position of the pad serves to nucleate domain walls directly in the structure. The left side of Figure 14 shows a SEM-image of the modified structure.

The GMR-curve of the sample is shown on the right side of Figure 14. The curve exhibits a lot of steps within, as well as a widening of the GMR-loop. Also the resistance is higher than in the structures before due to its greater length. The steps are caused by the pinning of the domain walls in the structure. The domain wall nucleation pad can act as an artificial pinning center for the walls in the structure in addition with imperfections in the longer structure, causing the steps in the curve.

A bias magnetic field near the steps was applied for the pulse measurements. The read pulses have a length of 500 ms at a current of 1 mA corresponding to a current density of $1.19 \cdot 10^{11}$ A/m². The write pulses have a length of 100 ms and a current density of $> 1.2 \cdot 10^{11}$ A/m² for positive, respectively $< -1.9 \cdot 10^{11}$ A/m² for negative magnetic fields. External bias magnetic fields of −81 Oe and 56 Oe were applied for the two measurements shown in Figure 14. The pulse measurements are plotted in the graph of the GMR-curve. In the curves the total resistance of the structure is plotted against the number of the stress pulses.

One increase from the initial state of resistance can be detected in the curve with an applied field of −81 Oe. For an external magnetic bias field of 56 Oe Figure 14 depicts a decrease over two steps. The resistance changes in steps corresponding to the steps in the GMR-curve. The course of the resistance for the pulse measurements is indicated by arrows. Intermediate steps are apparent between the initial resistance-state and the final state in the pulse measurements. This strongly supports the idea of a linear memristor with a resistance that can be adjusted using nanosecond pulses. Such a device can be used as a robust and

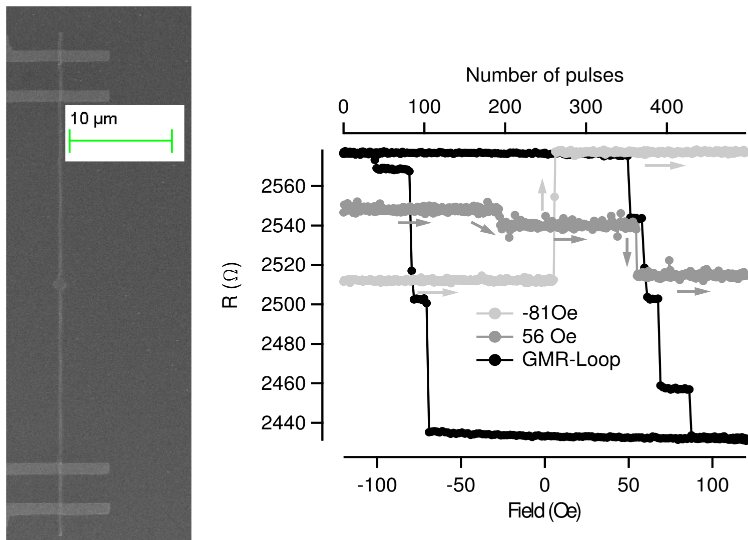

Figure 14: Left: SEM-image of the modified structure. The domain wall nucleation pad in the middle serves to create domain walls directly in the structure. Right: GMR-curve (black) of the sample with steps in it. The steps occur due to pinning centers in the stripe. The two other curves (grey) show the pulse measurements at an applied field of −81 Oe and 56 Oe. The resistance switches in steps corresponding to those in the GMR-curve. Intermediate steps between the initial and final resistance are visible. The course of the resistance for the pulse measurements is indicated by arrows.

fast component for application e.g. in artificial neural networks to mimic systems of neurons, or as sensors.

Resistive switching in memristive tunnel junctions and its application

The first realized memristor was based on resistive switching.[52] An insulating layer is, commonly, embedded within two conducting electrodes in a system that shows resistive switching. A drift of charge carriers, most likely oxygen or oxygen vacancies, takes place, if a voltage is applied. In these systems a change in the resistance caused by the charge carrier drift can be observed, depending on the applied voltage. The voltage has to exceed a critical threshold to cause a drift of charge carriers.

[52] D. Halley et al., Appl. Phys. Lett. **92** (2008) 212115; M. Janousch et al., Adv. Mater. **19** (2007) 2232–2235; P. Krzysteczko et al., J. Magn. and Magn. Mater. **321** (2009) 144 –147; D.B. Strukov et al., Nature **453** (2008) 30–83; J. M. Teixeira et al., J. Phys. D: Appl. Phys. **42** (2009) 105407; R. Waser and M. Aono, Nature Mater. **6** (2007) 833 –840; C. Yoshida et al., Appl. Phys. Lett. **92** (2008) 113508

The memristor developed by Strukov et al. consists of a Metal | Oxide | Metal crosspoint junction. The active element is a 5 nm thick oxide film that has an insulating TiO_2 layer in its initial state, as well as a layer of oxygen-poor TiO_{2-x}. Oxygen vacancies act as double positive charged dopants in this system. In an electric field the vacancies drift and move the boundary between TiO_2 and TiO_{2-x}, thus changing the resistance by heightening or lowering the effective barrier thickness.

Magnetic tunnel junctions

In the course of this chapter the resistive switching in magnetic tunnel junctions (MTJs) is examined. An MTJ basically consists of a trilayer composed of two ferromagnetic electrodes separated by a thin tunnel-barrier. If a bias voltage is applied, electrons tunnel from one ferromagnet into the other. The amplitude of the tunnel-current then depends on the relative magnetization orientation of the ferromagnets. The resistance is smallest in parallel and largest in antiparallel orientation of the electrodes. This effect was discovered in 1975 and is called tunnel magnetoresistance (TMR)-effect.[53]

[53] M. Julliere, Phys. Lett. **54 A** (1975) 225–226

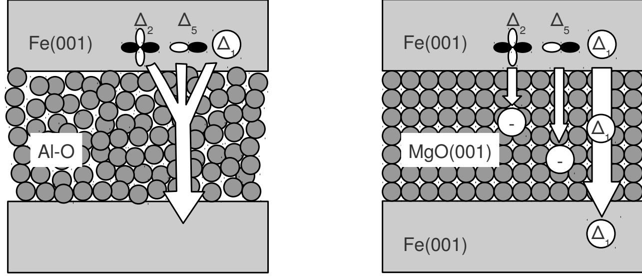

Figure 15: Sketch of electron tunneling through an amorphous AlO-barrier (left) and a crystalline MgO-barrier (right). Δ_1, Δ_2 and Δ_5 are Bloch states with different symmetries. The figure was reproduced from Yuasa et al. Journal of Physics D: Applied Physics **40** (2007) R337.

The Julliére-model is used for a simple explanation of this effect: The TMR-effect is caused by the spin of the conduction electrons in the ferromagnets, which is conserved during tunneling. Spin reversal processes like scattering in the barrier are not considered, since the spin-orientation of the electrons is conserved during tunneling.[54] The tunneling probability of each spin direction is proportional to the effective density of states (DOS) of the respective spin direction in the ferromagnetic electrodes. The spin-polarization is then defined as:

[54] P. M. Tedrow and R. Meservey, Phys. Rev. Lett. **26** (1971) 192–195

$$P := \frac{N_\uparrow - N_\downarrow}{N_\uparrow + N_\downarrow} \tag{17}$$

with $N_\uparrow$ the DOS of the majority electrons and $N_\downarrow$ the DOS of the minority electrons. The TMR-ratio then can be calculated by the spin-polarization of the ferromagnets:

$$TMR := \frac{2P_1P_2}{1 - P_1P_2} \tag{18}$$

with P_1 and P_2 the spin-polarization. In the Julliére-model, the spin-polarization is an intrinsic property of the electrode material. If a nonmagnetic material is used, the spin-polarization is $P = 0$. For a magnetic material with a fully spin-polarized DOS at the Fermi-energy is $|P| = 1$. The spins of the conduction electrons are brought into an alignment that differs from the normal distribution if a current flows through a ferromagnet. The electrons with a spin antiparallel to the magnet's orientation of magnetization will experience a higher scattering as well as spin-flip-processes. It is possible to calculate the TMR ratio based on

the actual measurement from the measured resistance in parallel ($R_{\uparrow\uparrow}$) and antiparallel ($R_{\uparrow\downarrow}$) case:

$$TMR := \frac{R_{\uparrow\downarrow} - R_{\uparrow\uparrow}}{R_{\uparrow\uparrow}} \tag{19}$$

Amorphous AlO barriers were studied extensively since the discovery of the TMR effect at room temperature in 1995.[55] In 2001 Butler, as well as Mathon and Umerski proposed the use of MgO as barrier material due to its crystalline structure.[56] Figure 15 shows two MTJs with Fe(001) electrodes as an example for a 3d-ferromagnet. The schematic illustration is reproduced from Yuasa et al.[57] The electrodes feature Bloch-states with different symmetries of the wave function. The completely symmetric Δ_1 Bloch-states have, generally, a high, positive spin-polarization in 3d-ferromagnets. In contrast the Bloch-states with lower symmetry like Δ_2 and Δ_5 often show a negative spin-polarization at the Fermi-energy.[58] The left MTJ in Figure 15 features an amorphous AlO barrier that naturally has no crystalline symmetry. Because of this unsymmetrical structure Bloch states with different symmetries can couple with states in the barrier which leads to a completely incoherent tunneling. The Δ_1 states are considered to have the highest tunneling probability which leads to a positive net spin-polarization. Because the other Bloch states also contribute to the tunneling process, the net is diminished which leads to a limited TMR-ratio.

[55] T. Miyazaki and N. Tezuka, J. Magn. Magn. Mater. **139** (1995) L231 – L2340; J. S. Moodera et al., Phys. Rev. Lett. **74** (1995) 3273–3276

[56] W. H. Butler et al., Phys. Rev. B **63** (2001) 054416; J. Mathon and A. Umerski, Phys. Rev. B **63** (2001) 220403; S. S. P. Parkin et al., Nature Mater. **3** (2004) 862 –867; S. Yuasa et al., Nature Mater. **3** (2004) 868 –871; S. Yuasa et al., J. J. Appl. Phys. **43** (2004) L588–L590

[57] S. Yuasa and D. D. Djayaprawira, J. Phys. D: Appl. Phys. **40** (2007) R337

[58] S. Yuasa and D. D. Djayaprawira, J. Phys. D: Appl. Phys. **40** (2007) R337

The right MTJ has a crystalline MgO(001) barrier. Here, in contrast to AlO, the tunneling probabilities depend on the symmetry of the Bloch-states. The Δ_1 states have higher probabilities of tunneling than the Δ_2 and Δ_5 since the Fe Δ_1 can couple with the MgO Δ_1 states. The Δ_1 states decay slowest in the barrier which leads to a high positive net spin-polarization and therefore a high TMR. TMR ratios of up to 600%[59] (1000% are predicted by Butler, Mathon and Umerski) can be reached with MgO based tunnel junctions compared to the limited TMR ratios of up to 70% in amorphous AlO MTJs.[60]

[59] S. Ikeda et al., Appl. Phys. Lett. **93** (2008) 082508

[60] Y. Huai et al., J. Magn. Magn. Mater. **304** (2006) 88 –92

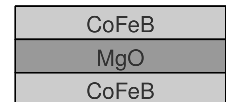

Figure 16: A trilayer of CoFeB | MgO | CoFeB as 'active' element is used for the measurements.

Memristive switching in magnetic tunnel junctions

A trilayer of CoFeB | MgO | CoFeB was used for the measurements. The investigated MTJs were fabricated by sputter deposition.[61] The MTJs have to be annealed at temperatures of around 375^oC

[61] A. Elshabini-Riad and F. D. Barlow III, McGraw Hill, 1998; J. A. Venables, Cambridge University Press, 2000; K. Wasa and S. Hayakawa, Noyes Publications, 1992

to get a crystalline MgO-barrier, thereby developing a crystalline barrier as shown on the right side of Figure 15.

Oxygen vacancies can accumulate on the interface between the lower electrode and the MgO-barrier, during the fabrication process. These oxygen vacancies start drifting on the interface between barrier and the bottom CoFeB if a voltage that exceeds the critical threshold is applied to this system. In MgO-based MTJs the resistance is highly dependent on the state of the interface between the barrier and the electrodes. Disturbances such as amorphous disorder in the crystalline structure effect the tunneling process and can, therefore, influence the resistance. The drifting of the oxygen vacancies changes the structure of the interface and therefore the resistance.

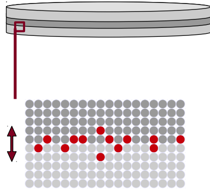

Figure 17: Simple model of the resistive switching in the memristive MTJs.The change in resistance is caused by drifting charge carriers at the interface of barrier and bottom electrode.

A simple model of the resistive switching in MTJs is shown in Figure 17. The image section of the MTJ shows the interface between barrier and lower electrode. It is supposed that the drifting of the charge carriers takes place only within a few monolayers at the interface. This model is supported by experiments on the same layer stack that had a post-oxidized tunnel barrier. These samples showed no memristive effects at all.[62] The effective barrier thickness is either raised or diminished by the drift of the oxygen vacancies, hence the change in the resistance. The effect of the resistive switching is defined analog to the TMR ratio as:

$$RS := \frac{R_{high} - R_{low}}{R_{low}} \tag{20}$$

Here R_{high} is the HRS and R_{low} the LRS.[63]

[62] P. Krzysteczko, G. Reiss and A. Thomas, Appl. Phys. Lett. **95** 112508(2009) 112508

[63] P. Krzysteczko, Dissertation, Universität Bielefeld, 2010

Methods and measurements

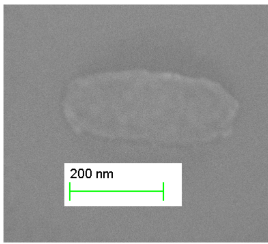

Figure 18: SEM-picture of an elliptic MTJ with axes of 300 nm and 150 nm.

The investigated TMR systems were provided by Singulus. They were fabricated by sputter deposition in a Singulus TIMARIS II tool and have the following layer stack: Ta 3 | Cu-N 90 | Ta 5 | $Pt_{37}Mn_{63}$ 20 | $Co_{70}Fe_{30}$ 2 | Ru 0.75 | $Co_{66}Fe_{22}B_{12}$ 2 | MgO 1.3 | $Co_{66}Fe_{22}B_{12}$ 3 | Ta 10 | Cu 30 | Ru 7 (all thicknesses in nanometer). The MTJs are structured to elliptical pillars by e-beam-lithography and ion beam etching. In the first preparation step the ellipses are written in the negative e-beam resist. Afterwards the sample is etched and filled up with the insulator Ta_2O_5. After the removal of the resist and the oxide on top of the MTJs, 6 nm of Ta and 35 nm Au are sputtered on top. The contact-pads are structured in the second lithography step in these layers. The formed ellipses have

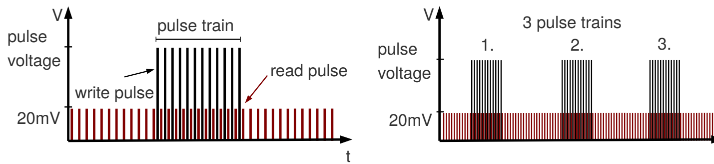

Figure 19: Left: Sketch of the measurement method. To initialize the resistive switching write pulses alternating with read pulses are applied to set and determine the resistance. A series of read pulses is called a pulse train. Right: Series of three pulse-trains applied to the MTJ.

axes of 300 nm and 150 nm. An SEM-image of an MTJ is shown in Figure 18. It was taken after the removal of the resist and the insulator. The details concerning the structuring can be found in the *Appendix*.

A critical voltage of approximately 300 mV to 400 mV has to be applied (as can be seen on the right side of Figure 21) to cause the drift of oxygen vacancies. An alternating series of read and write pulses (also called stress pulses) is applied as shown in Figure 19 to measure the resistive switching. The envelope function of the write pulse can have an arbitrary form, like a sine as in Figure 20. However, the shown method of alternating read and write pulses is always the same. A series of write pulses is called a pulse-train, as depicted in Figure 19. The write pulses are set to zero to monitor the resistance before and after the stress pulse. All measurements were performed at room temperature. Also, for all experiments the bottom electrode is grounded as measurement convention. That implies that for a positive bias voltage the electrons flow from the bottom to the top electrode. According to this, the assumed oxygen vacancies move at the interface between bottom electrode and barrier, in- and decreas-

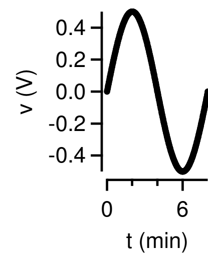

Figure 20: Sinusoidal stress voltage applied to the MTJ to measure the memristive loop.

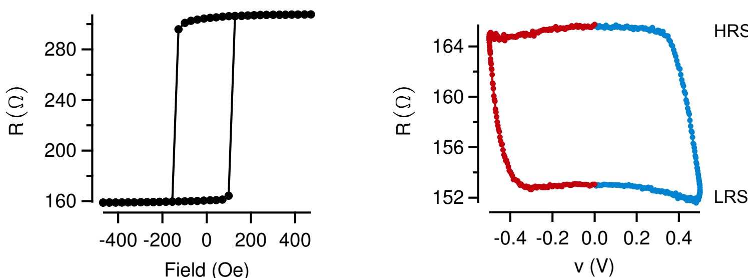

Figure 21: Left: Typical resistance-curve of a TMR measurement in a memristive MTJ. The TMR effect of the elements is about 100%. Right: Memristive curve of a MTJ stressed with a maximum voltage of 500 mV. The device shows an effect of 8%.

ing the effective barrier-thickness. Since a pristine memristive MTJ is in an undefined resistance-state before the actual measurement, the elements are stressed, so that the measurement can start from a defined resistance. This is either the HRS or the LRS. The TMR effect of the elements is about 100% while the resistive switching has an amplitude of up to 8%. The resistance curves of both measurements are shown in Figure 21. A sinusoidal stress voltage was applied at the MTJ as shown in Figure 20, for the measurement of the memristive effect.

[64] P. Krzysteczko, Dissertation, Universität Bielefeld, 2010

Large parts of the characterization of memristive MTJs were already done by Krzysteczko.[64] As a result, in this thesis the attention is more focused on characteristics that allow applications of the effect. It is useful to know the voltage and pulse time dependence of such a device to tailor the resistance of an MTJ. The memristive change in resistance was initiated using a series of ten write pulses with a length of 1 s each. The current was measured during 200 ms read pulses at a read-out voltage of 20 mV to determine the resistance. A constant external magnetic field of 0.04 T was applied during the measurements to stabilize the parallel magnetic state. Three pulse-trains were applied for

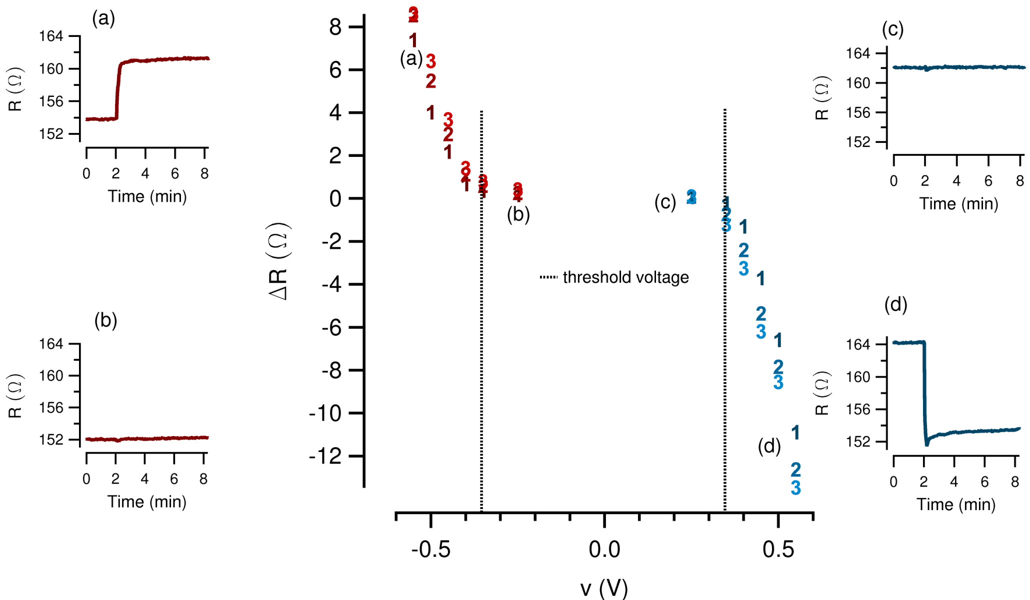

Figure 22: Resistance change ΔR as a function of the applied pulse-train voltage. Overall, three pulse trains are subsequently applied for every voltage. The resistance change after the first, second and third pulse train is labeled 1,2, and 3, respectively. The insets show the change in resistance after applying one pulse. The pulse-train was always initiated after two minutes (cp. insets).

every voltage as shown in Figure 19 and the resistance change was determined. The memristor was reset to its former value with a voltage pulse of the opposite sign, after completing the measurements.

The results are shown in Figure 22. The resistances after the first, second and third pulse-train are marked with the numbers 1, 2, 3. From the data, the threshold voltage is estimated at approximately 300 mV. Whenever the applied voltage exceeds this limit, a resistance change can be detected. The four insets highlight the changes in resistance from four voltages of −550 mV, −250 mV, 250 mV and 550 mV. The scale of the resistance in all four insets is identical. It can be seen that there is no change in the resistance course for the voltages below the threshold. The results shown in the graph also indicate that it is possible to target a certain resistance-state by applying either a series of pulse-trains with smaller amplitudes or a single pulse-train with a larger amplitude. This sample exhibited a maximum change in resistance of approximately 13 Ω (or 8%).

The stability of the targeted resistance-state is another interesting benchmark for application. An MTJ with an initial resistance of approximately 173 Ω was stressed with a voltage pulse of −500 mV to a resistance of 175 Ω. The resistance of the stressed device was measured at a low monitoring voltage and no change in the resistance could be detected over the time of six hours. This is evidence of the long term stability of the system.

Furthermore the dependence of the resistance change ΔR on the duration of the stress pulse is determined. A memristive MTJ is stressed with voltages of ±550 mV or this measurement. These voltages are applied for times of 0.2 s, 0.5 s, 1 s, 5 · 1 s and 10 · 1 s. Two consecutive pulse-trains with different lengths are applied for the measurement. After each measurement the

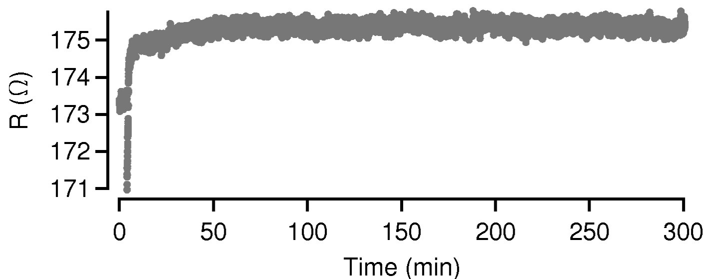

Figure 23: Long-term measurement of the resistance of an MTJ after stressing with −500 mV. The element shows no signs of relaxation after six hours.

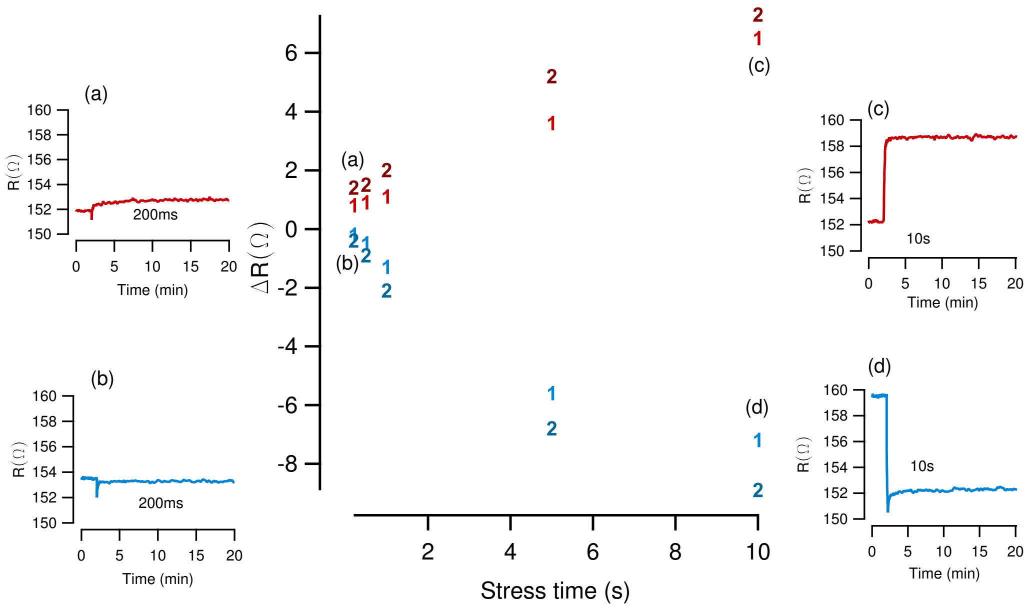

Figure 24: Resistance change ΔR as a function of the stress pulse duration. The stress voltage is kept constant at ±550 mV. Overall, two pulse trains are subsequently applied for every stress time. The resistance change after the first and second train is labeled 1 and 2, respectively. The insets show the change in resistance after applying one pulse.

memristor was reset by a voltage pulse of the opposite direction. The results are shown in Figure 24. The insets show the change in resistance after applying one pulse. ΔR has a smaller rising for the negative voltages than decay for positive voltages. For short pulses ΔR is rather small, which would allow a fine tuning of the resistance. Also, it stands out, that the system by now has a rather long reaction time to the stress pulses. That behavior still is a challenge for optimization towards shorter operation times. Anyway, the memristive effect in MTJs can be used to improve the error tolerance in the next generation of magnetic random access memory (MRAM) and, more interesting field programmable gate arrays (FPGAs), because the memristance compensates for the resistance fluctuations.

Application in FPGAs

The application of MTJs to MRAM and FPGAs was hypothesized, when TMR was observed at room temperature, due to the high and low resistance-states they exhibit in dependency on the orientation of the electrodes.[65] The concept of a FPGA entails that

[65] D. Meyners et al., J. Appl. Phys. **99** 023907; G. A. Prinz, Science **282** (1998) 1660–1663; G. Reiss and D. Meyners, Appl. Phys. Lett. **88** (2006) 043505; R. Richter et al., Appl. Phys. Lett. **80** (2002) 1291–1293; Jr. W. C. Black and B. Das, J. Appl. Phys. **87** (2000) 6674–6679

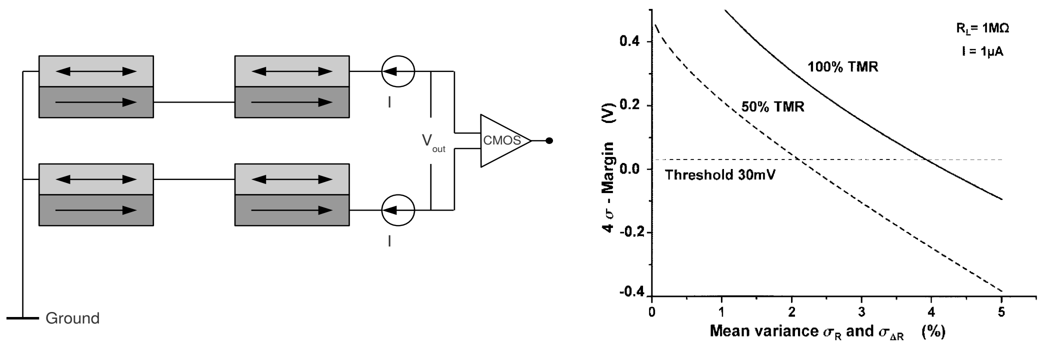

Figure 25: Left: Sketch of an FPGA consisting of four MTJs which are connected to two current sources. The voltage V_{out} is the logic output which is amplified by a CMOS circuit. Right: Consideration on the error tolerance of MTJ based FPGAs. The figure was taken from G. Reiss and D. Meyners, Appl. Phys. Lett. **88** (2006) 043505

the logic input into this device is stored in a minimum of two MTJs. Additionally, two further MTJs define the logic function of the gate. The programming and the input are done by switching the magnetic orientation of the MTJ between the parallel and antiparallel state. These states can be associated with the logical values zero and one. However, it has been shown that fluctuations in the resistance of the junctions limit their use in FPGAs.[66] The acceptable level of resistance variation depends on the TMR ratio of the junctions.

Distinguishing between high- and low-resistance-states is not possible once these variances exceed certain values. As mentioned above, common magnesium-oxide-based MTJs exhibit high TMR values of up to 600%, [67] but industrially fabricated MRAM and FPGA devices rarely feature TMR ratios above 100%.[68] The recently proposed spin transfer torque-MRAM (STT-RAM) requires a thin barrier and low resistance.[69] [70] This results in a TMR ratio of at maximum 160% for current induced magnetization switching.[71] Also, amorphous AlO-barriers are still often used, as well as electrodes that are optimized for their magnetic switching behavior rather than their suitability for a high TMR ratios. The variations in the junction resistance are due to either thickness fluctuations in the tunnel barrier or to variability in the junction sizes caused by the lithography process. These resistance fluctuations are of the same magnitude as the memristive effect observed in the MTJs. In other words, the fluctuations can be counterbalanced using the memristive properties of the investigated MTJs.

In Figure 25 a sketch of an FPGA is pictured on the left side.

[66] compare to G. Reiss and D. Meyners, Appl. Phys. Lett. **88** (2006) 043505

[67] S. Ikeda et al., Appl. Phys. Lett. **93** (2008) 082508

[68] R.W. Dave et al., Magnetics, IEEE Transactions on **42** (2006) 1935 –1939

[69] J. Åkerman, Science **308** (2005) 508–510; M. Hosomi et al., in, Electron Devices Meeting, 2005. IEDM Technical Digest. IEEE International, 2005, 459 –462; J. C. Slonczewski, J. Magn. Magn. Mater. **159** (1996) L1 –L7

[70] J.A. Katine and Eric E. Fullerton, J. Magn. Magn. Mater. **320** (2008) 1217 –1226

[71] Y. Huai et al., J. Magn. Magn. Mater. **304** (2006) 88 –92; D. H. Lee and S. H. Lim, Appl. Phys. Lett. **92** (2008) 233502; S. Yuasa et al., Nature Mater. **3** (2004) 868 –871

On the right side the consideration about the error tolerance in MTJ based FPGAs is shown. A voltage difference of about 30 mV has to be exceeded to differentiate between certain resistance levels, for an implementation on complementary metal-oxide-semiconductor (CMOS) technology.

For MTJs with an effect amplitude of 100% the mean variance of the resistance, respectively the resistance change, has to be smaller than 4% to reach that threshold. The variances in the resistance tend to be between 3% and 6%. Further analyses were performed on similar MTJs by tuning two different junctions to the same resistance to show that it is possible to counterbalance these fluctuations. The results are shown in Figure 26, which depicts the absolute resistance of the MTJs. As above, pulse-trains with different amplitudes were applied, and the resulting resistances were subsequently measured. The results indicate that it is possible to drive two MTJs with different initial resistances to similar final resistances, as long as the fluctuations in the FPGAs are not larger than the memristive effect. The area between the dotted lines represents the resistance overlap for both MTJs.

A resistance variation of 1.2% was targeted. That corresponds

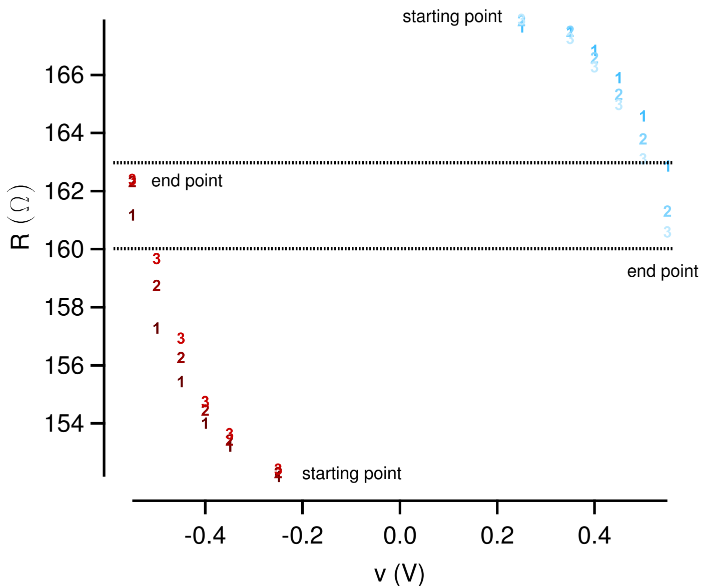

Figure 26: Total resistance of two MTJs with different initial resistances. The left curve and the right curve represent resistance characteristics while stressing the first and the second MTJs with three consecutive pulse-trains of variable bias for each datapoint. The area between the dotted lines represents the resistance overlap for both MTJs

to a voltage difference in FPGAs of approximately 450 mV (compare to Figure 26). This is above the threshold for reliable operation of 30 mV.

In brief summary, the potential of memristive MTJs for the optimization of MRAMs and magnetic FPGAs has been discussed. It has been shown that it is possible to tailor the resistances of these devices and thus compensate for resistance fluctuations that occur as a result of the fabrication process. The MTJs maintain stable resistances and do not need to be periodically refreshed. An additional reset cycle needs to be implemented for application in STT-MRAM, because the high current densities necessary for operation will inevitably also trigger the resistive switching.

Application of memristive MTJs in artificial neuronal systems

Since the recent successful implementation of the long-hypothesized memristor, its use in neuronal computing and in the reproduction of biological neural networks has gained increasing attention. Before the neuronal characteristics of memristive MTJs are addressed, an introduction into the biological prototype and its characteristics is given.[72]

[72] Campbell, Peason Education, 2011; T. P. Trappenberg, Oxford University Press, 2010

About biological neuronal systems

Figure 27 shows the sketch of a neuronal system with its main features. The nucleus of the cells is neglected for simplicity. The system consists of a presynaptic cell and a postsynaptic cell. Between them, the way of a hypothetical stimulus is drawn from the presynaptic to the postsynaptic cell. A number of branched dendrites is connected to every cell body, receiving signals from other neurons. Also a single axon is connected to the cell body, it transmits signals to other cells via the synapses. The synapses are another crucial part of a neuron. There are two kind of synapses, electrical and chemical synapses. The electrical synapses have faster response times but, in general, are not able to amplify the signal and either transmit it completely or not at all. Only recently some of the electrical synapses showed evidence for strengthening or weakening of the electric connection as response to activity in the synapse.[73] The electric synapses are neglected during the course of this chapter due to their generally binary nature. Chemical synapses form the junction where the transmitted signals enter the synaptic terminal, where information is passed by chemical agents, so called neurotransmitters as can be seen in the image section. The signal genesis, synthesis and processing also have to be dealt with, besides the design of a neuronal system.

[73] J. S. Haas, B. Zavala and C. E. Landisman, Science **334** (2011) 389–393

In a biological system of cells, ions are unequally scattered

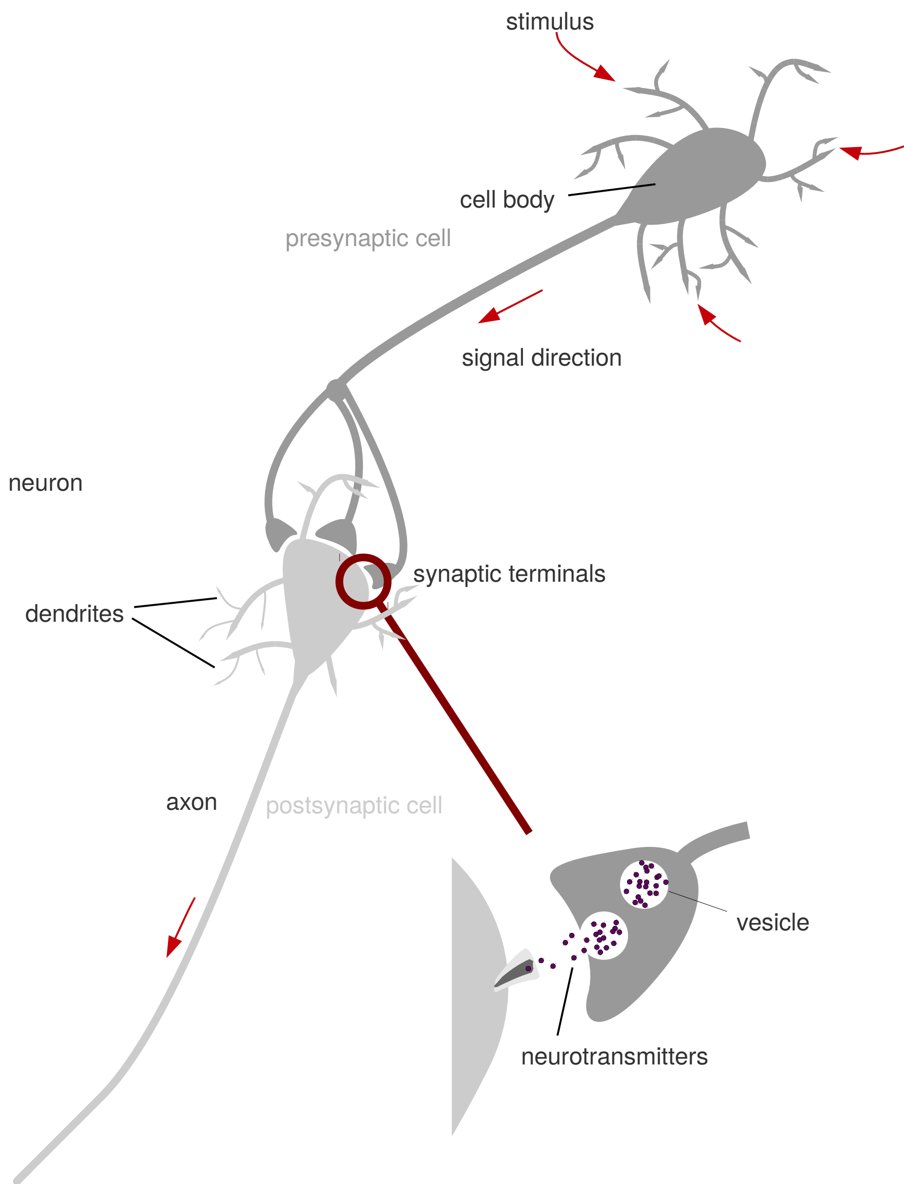

Figure 27: Sketch of the neurons structure and its organization. In the synapse neurotransmitters are synthesized and stored in the vesicles. They serve as chemical messengers and are removed after use by diffusion and degradation.

between the inner cell and the surrounding liquid. This leads to a negative charged interior in respect to the outside. This charge difference or voltage is called membrane potential. For a resting neuron it is also called the resting potential, with typical voltages between −30 mV and −80 mV. The membrane potential can be changed by inputs and stimuli from other neurons. It acts as a signal to transmit and process information. K^+ and Na^+ ions are the essential agents for the formation of the resting potential. The gradients of concentration are maintained by pumps and ion channels within the cells membrane. The membrane potential can be changed by a stimulus causing a higher negative charge (hyperpolarization) or a decrease of the potential (depolarization). One of the responses to such a polarization is a so called *graded potential*. It has a varying magnitude depending on the strength of the stimulus. The larger the stimulus, the larger the change in the membrane potential becomes. Graded potentials result in a small current flow along the membrane, thus decaying with distance from their origin.

While these potentials are not the actual nerve signal, they affect the generation of the nerve signals. They can be summed up due to their localized nature. A massive change of the potential occurs, if the depolarization shifts the membrane potential over a certain threshold (−55 mV for mammalian neurons), which is called *action potential*. Action potentials show a constant magnitude independent of their trigger and do not decay over distance. Therefore they can propagate along the axons and transmit signals over long distances. Since action potentials are only excited if the membrane potential exceeds the critical threshold, they are a one-or-nothing response to stimuli. The mechanisms of how action potentials are generated were explored by Huxley and Hodgkins in the 1940s and 50s.[74]

[74] A. L. Hodgkin and A. F. Huxley, J. Physiol. **117** (1952) 500–544

The potentials inevitably cause electric activity at the synapses, while traveling through the neuron, since they can not propagate further directly. To cross the synaptic terminals the signal has to be conversed into a chemical signal by releasing neurotransmitters into the gap of the synaptic terminal. These agents lead to an intermittent transmissibility of the membrane proteins on the postsynaptic side in order to transmit the action potential. This activity can, in general, cause a lasting increase or decrease of the synapses efficiency. These modifications are called long term potentiation (LTP) and long term depression (LTD). This plasticity is considered an essential element for learning and memory processes.

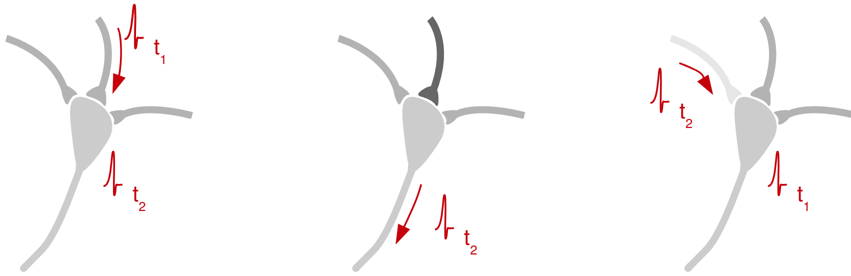

Figure 28: Sketch of the course of STDP: An action potential of the presynaptic side arrives at t_1 at the synapse. Left: Stimulus exceeds the threshold and causes a response which results in an action potential at t_2. Middle: Propagating action potential that is also acting on synapses in backward direction. Here $t_2 > t_1$ which results in strengthened connection (darker grey). Right: Reversed timing $t_2 < t_1$, thus the connection is weakened (lighter grey).

While the idea that the brain is changing and adapting by building associations is not particularly new, it was first coherently described by Hebb in 1949.[75] He proposed that cell assemblies in the brain form dynamically in response to external stimuli and that this builds the main part of information processing in the brain. The basic physical mechanisms are synaptic changes. The central component of his work was the significant correlation between presynaptic and postsynaptic activity which can be summed up with the Hebbian rule: *what fires together wires together*. The concept that activity dependent plasticity is based on pre- and postsynaptic activity is referred to as *Hebbian plasticity* or *Hebbian learning*. Classic plasticity experiments utilize high frequency presynaptic stimulation to get LTP and low frequency for LTD. The stimulus has to be strong enough to excite the postsynaptic neuron, thus reflecting the Hebbian rule that there is a causal relation between presynaptic and postsynaptic spikes. Newer experiments further investigated the causal relation between pre- and postsynaptic spiking by varying the time between the externally induced pre- and postsynaptic spikes. This principle of spike timing dependent plasticity (STDP) is shown in Figure 28. [76] The image depicts the mode of operation of STDP. An action potential reaches the presynaptic side of a neuron at the time t_1. The left picture shows the depolarizing response that is caused by the stimulus. It leads to an action potential on the postsynaptic side at time t_2. The image in the middle shows the propagation of the signal along the axon while also acting on the synapses in backward direction. Here $t_2 > t_1$ which leads to a strengthened connection indicated by the darker grey. The right

[75] D. O. Hebb, 1949

[76] C. C. Bell et al., Nature **387** (1997) 278 –281; J. C. Magee and D. Johnston, Science **275** (1997) 209–213; H. Markram et al., Science **275** (1997) 213–215

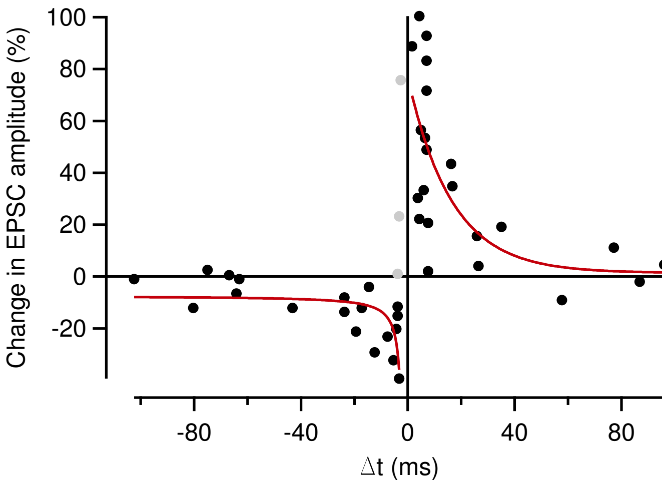

Figure 29: Reproduction of the biological STDP data from Bi et al., Journal of Neuroscience, **18** (1998) 10464–10472. The critical window for the induction of synaptic potentiation and depression is at $\Delta t = \pm 40$ ms. The curve was fitted with equation 21.

picture shows the situation with reversed timing $t_2 < t_1$ which weakens the connection indicated by the lighter grey. The actual measurements of the asymmetric STDP are shown in Figure 29. The data was reproduced from Bi et al.[77] The graph shows the relative changes of the excitatory postsynaptic current (EPSC) for different values of the time interval Δt between pre- and postsynaptic spikes.[78] It also illustrates that there is a critical time window around $\Delta t = 40$ ms. No STDP occurs, if the absolute values of the time interval grow larger than this. Changes are largest for small positive and negative time intervals between pre- and postsynaptic spike times.

[77] G. Bi and M. Poo, J. Neurosci. **18** (1998) 10464–10472

[78] B. Berninger and G.-Q. Bi, BioEssays **24** (2002) 212–222

The biological data shows a lot of noise. Despite this, the course of the datapoints is fitted to the following equation:[79]

[79] S. Song, K. D. Miller and L. F. Abbott, Nature Neurosci. **3** (2000) 919 –926

$$F(\Delta t) = \begin{cases} A_+ \exp(\Delta t/\tau_+) & \text{if } \Delta t < 0 \\ -A_- \exp(-\Delta t/\tau_-) & \text{if } \Delta t \geq 0 \end{cases} \tag{21}$$

Here the parameters τ_+ and τ_- determine the ranges of pre- to postsynaptic inter-spike intervals over which the synaptic strengthening and weakening occurs. A_+ and A_- are the maximum amplitude of synaptic modification, when Δt is close to zero. Those equations are used to provide a model for e.g. computational neuroscience and fit the decay of change of EPSC reasonably well. For the fit, the data points for negative Δt close to zero were excluded since the variations were too large to pro-

vide even a qualitative fit. The excluded points are marked in grey. After describing the bases of the biological system, now the neuronal characteristics of the memristive MTJs can be dealt with.

Spike timing dependant plasticity in memristive MTJs

At first it is necessary to find analogies between the biological system and the MTJs. The working principles are rather different. In the biological system, the signals are transmitted by the release of neurotransmitters in the cleft of the synaptic terminal. The memristive MTJs utilizes the drift of oxygen vacancies to change its resistance-state. However, the common characteristics can be compared. First, both systems have certain thresholds above which they activate. That is the action potential for the synapse and the critical voltage for the memristor. Furthermore, it is more graphic to start with the basics of STDP, namely LTD and LTP, than STDP itself. The LTD and LTP in a mice neuron are plotted

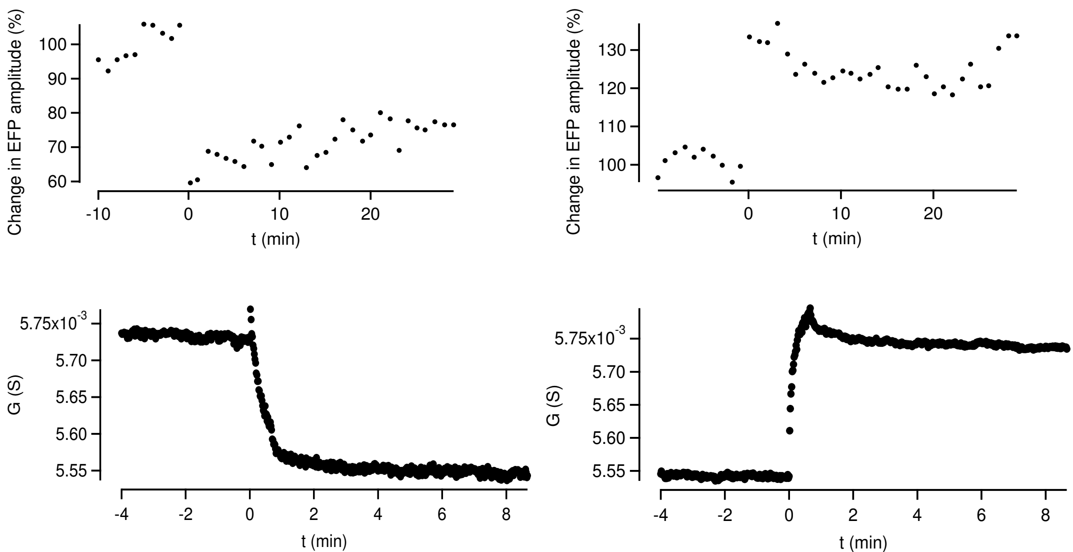

Figure 30: Plot of LTD and LTP in synapses from mice neurons in comparison with the analog parameter in the memristive MTJs. The upper measurements show the change of EFP amplitude compared to the averaged initial state ($t = -10 - 0$ min). At $t = 0$ min the neuron was stressed by a low frequency stimulus for LTD, respectively a high frequency stimulus for LTP. The data was reproduced from Dang et al., PNAS, **103** (2006) 15254–15259. In the graphs below, as for the biological measurements, the initial state of the memristor before the stimulus is monitored for $t = -4 - 0$ min. After four minutes the element was stressed by a voltage pulse of ∓ 500 mV and the change of electric conductance can be detected.

in the upper graphs of Figure 30. The data was taken from Dang et al.[80]

[80] M. T. Dang et al., PNAS **103** (2006) 15254–15259

The measurements show the change of evoked field potential (EFP) amplitude compared to the averaged initial state ($t = -10 - 0$ min). At $t = 0$ min the neuron is stressed by a low frequency stimulus for LTD, respectively a high frequency stimulus for LTP. A decrease in the change of EFP amplitude can be seen for the LTD, corresponding to a reduced signal transmission of the neuron. The opposite case of LTP shows an increase of the change of EFP amplitude, effectively enhancing the signal transmission.

Unlike before the resistance of the memristor might not be the best suited parameter for comparison in this case. A high resistance is correlated to a decreased current signal, so the use of HRS and LRS might lead to confusion. The inverse of the resistance, the electric conductance is employed for this reason since it is directly proportional to the measured current signal. The graphs in Figure 30 show the memristive analogy to LTD and LTP. As for the biological measurements, the initial state of the memristor before the stimulus is monitored for $t = -4 - 0$ min. After four minutes the element was stressed by a voltage pulse of ∓ 500 mV.

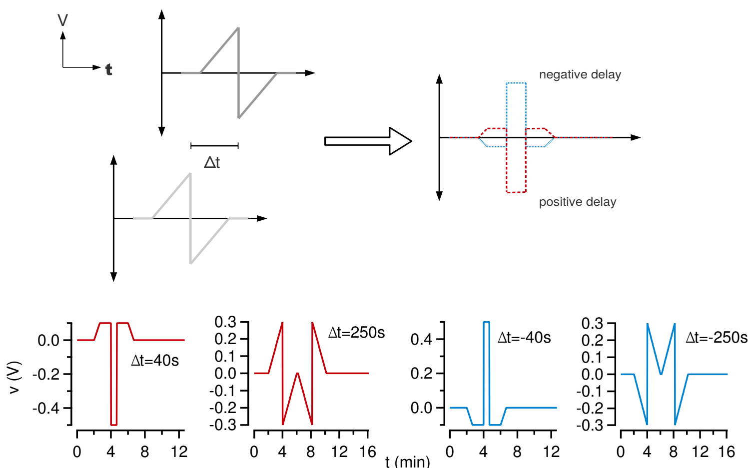

Figure 31: Sketch of the pulse generation for STDP. Two sawtooth pulse-trains are superposed with a temporal delay that can either be positive or negative. The plotted insets show the envelopes of the pulse-trains that were applied to the memristive MTJs. The initial pulses have an amplitude of ±300 mV. This amplitude is just below the critical threshold. The amplitude of the morphed pulses falls below the threshold for large delays and the initial pulse-forms become recognizable. The small insets show the morphed pulses for small (±40 s) and large (±250 s) delays.

The curve of the resulting change in the electric conductance resembles the biological measurements in both cases.

A python script is used to superpose two sawtooth signals with a varying temporal delay in between them to simulate the STDP. The sawtooth pulses are identified with the incoming pulses on the synaptic side. Figure 31 shows the envelope of the initial pulse-train and the resulting morphed pulse-form. As before the pulse-trains consist of alternating read and write pulses. The initial pulse-trains have an amplitude of ±300 mV. This is a value just under the critical threshold. The superposed pulse-form corresponds to the summed up signal on the synapse. The height of the morphed pulse-trains depends on the delay between the initial pulse-trains. The insets of Figure 31 show four morphed pulse-trains as applied to the memristive MTJs with a positive delay of ±40 s and ±250 s. As can be seen, the longer the delay, the smaller the amplitude of the morphed pulse-trains becomes. For large delays the amplitude falls below the threshold voltage. In this case no LTD/LTP equivalent can be measured in the memristor and the initial pulse-trains become visible in the morphed pulse-trains again.

Figure 32 shows the results for the STDP measurements in memristive MTJs (cp. P. Krzysteczko et al.).[81] The memristor is stressed with morphed pulse-trains for different temporal delays. For every delay three pulse-trains are applied and the change in

[81] P. Krzysteczko et al., Adv. Mater. (2012) 762–766

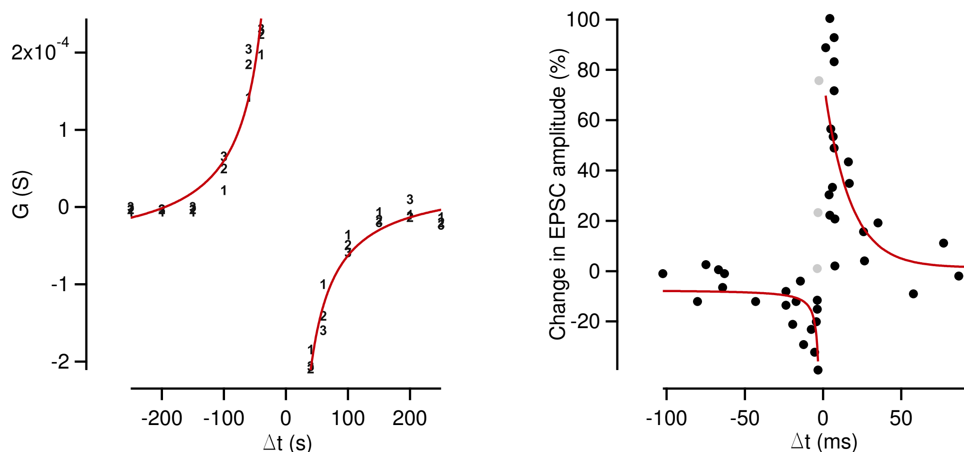

Figure 32: Left: STDP in memristive MTJs. A memristive MTJ is stressed with three consecutive morphed pulse-trains for each temporal delay, varying from ±40 s to ±250 s and the change in the electric conductance is determined. The electric conductance value after the first, second and third pulse-train is labeled 1,2, and 3. The device is reset by a voltage pulse of the opposite direction after three pulse-trains. The data points are fitted with equation 21. Right: In comparison, the biological curve for STDP.

the electric conductance is determined. The electric conductance value after the first, second and third pulses train is labeled 1,2, and 3. After three pulse-trains the device was reset by a voltage pulse of the opposite direction. The biological curve of STDP is plotted next to the electric conductance curve of the memristive MTJ in comparison. The electric conductance curve is tilted by 90° compared to the biological curve. This is due to the measurement convention: The bottom electrode is grounded for all experiments on memristive MTJs in this thesis to avoid confusion. Reversing the polarity of the contacts would result in the biological curve.

Like the STDP curve in nature there is a critical delay between the initial pulse-trains: No change in conductance and resistance can be detected for delays over $\Delta t = 100\,\mathrm{s}$. The curves are fitted with the same function of equation 21. Here τ_+ and τ_- are the ranges of intervals over which the conductance changes occur. A_+ and A_- are the maximum amplitudes for small Δt. Figure 32 shows that the equation provides a reasonably good approximation for the obtained data. The measurement also shows only low random noise.

In summary, it is possible to detect synaptic characteristics in single memristive MTJs. The MTJs show effects like LTD and LTP as well as STDP-like behavior that makes them interesting for application in artificial neuronal systems.

Coupled system with exhibitory and inhibitory characteristics

While the idea that there is neuronal behavior in single memristor systems is intriguing, one neuron or synapse alone does not lead to higher brain functions. While there are protozoons like the amoeba-like slime mold Physarum polycephalum that show a primitive learning behavior[82] with regard to their mobility in cold and hot environment, in general higher organisms do not function with only one neuron. So, if complex organisms are to be emulated it is necessary to investigate not only single memristors but systems of coupled MTJs. These systems can later be expanded to artificial neural networks based on coupled memristors.

[82] Y. V. Pershin, S. La Fontaine and M. Di Ventra, Phys. Rev. E **80** (2009) 021926

If two memristors are series-connected, the resistance adds up like in a normal series connection:

$$R_{tot} = \sum_{i=1}^{n} R_i \tag{22}$$

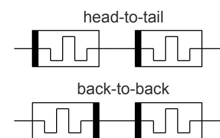

Figure 33: Configurations of two memristors.

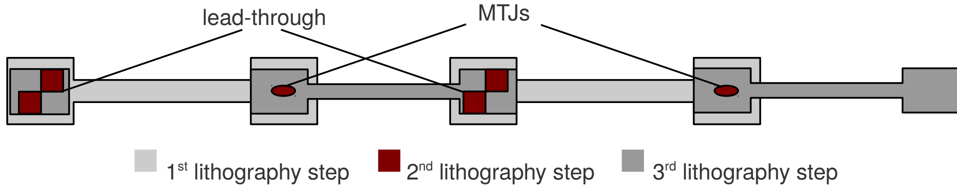

Figure 34: Sketch of the layout for the three-step-lithography of the head-to-tail-system. The elliptic MTJs written in the second step are not true to scale.

Analog the total resistance of a parallel connection calculates to:

$$\frac{1}{R_{tot}} = \sum_{i=1}^{n} \frac{1}{R_i}. \tag{23}$$

As was pointed out before, the direction of the connection must be considered. This is especially important for coupled memristive systems. The oxygen vacancies are supposed to be located at the interface between bottom electrode and barrier.[83] This fact has to be considered in coupled memristive systems. It has to be discerned between two configurations that are shown in Figure 33. The first configuration can be referred to as *head-to-tail*. This system shows the known memristive characteristics in the resistance when stressed, once the voltage reaches the critical threshold. The second possible configuration is called *back-to-back* in the following. Here the total resistance passes into an equilibrium state if the system is stressed. This system is dominated by the memristor with the higher sensitivity to the applied voltage. The back-to-back system is only interesting as a neutral element.

[83] P. Krzysteczko, G. Reiss and A. Thomas, Appl. Phys. Lett. **95** 112508(2009) 112508; P. Krzysteczko et al., J. Magn. and Magn. Mater. **321** (2009) 144 –147

A three-step-lithography has to be performed for the head-to-tail system to connect the MTJs in the correct direction. A sketch of the basic layout for the head-to-tail configuration is shown in Figure 34. In the first step the conduction paths and contact pads for the bottom contacts of the two MTJs are written. The elliptic MTJs themselves are written in the second step. The ellipses in Figure 34 are not true to scale, but drawn bigger for visibility reasons. The upper contact lines and contact pads are written in step three. The contact pad in the middle allows to check both MTJs independently for functionality.

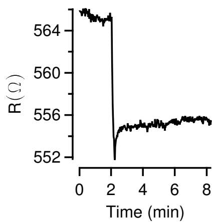

Figure 35: Resistance change in a coupled system after stressing with a single pulse-train with an amplitude of 1100 mV.

Figure 35 shows the change in the total resistance of a coupled system with parallel orientation of the electrodes that has been stressed by a pulse-train. The curves resemble those of sin-

gle memristors, while the resistance sums up after equation 22. Here, the resistance of a single memristive MTJ is approximately 275 – 300 Ω in the parallel state. The threshold voltage also rises with this higher resistance. For the measurements below the coupled system is stressed with 1100 mV. The resistive switching in this system is interesting to obtain a small change in the resistance, that can serve as signal. It is, however, not perfectly suited to emulate connected and disconnected strings of neurons in a network, due to its small amplitude. The TMR in the memristive MTJs can be utilized for this. As described in the chapter above, MTJs exhibit a parallel and antiparallel state of magnetization of the electrodes corresponding with high and low resistance. While the easiest way to switch an MTJ is to apply an external magnetic field, this approach is not useful in this case as it would switch the complete coupled system. Another approach is to structure conduction paths (write lines) over the elements and use the Oersted field of those paths for switching, which would allow a selective switching of single elements. The most convenient way, however, is to make use of the ultra thin 1.3 nm thick

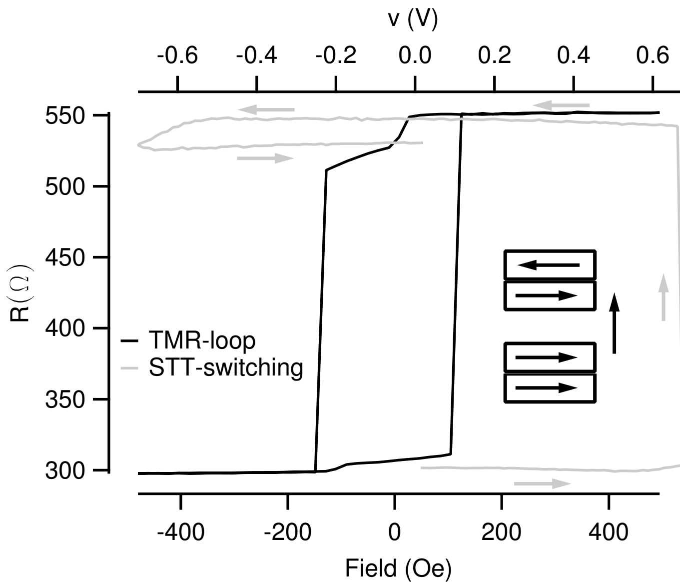

Figure 36: STT-Switching and the TMR-loop in a memristive MTJ. The graph shows the course of the resistance curve versus the applied voltage for STT-switching and the magnetic field for the TMR-loop, respectively. The right picture shows the STT resistance curve and the magnetic loop of the MTJ.

barrier of the MTJs and use spin transfer torque (STT)-switching.

The mechanisms of STT-Switching are closely related to those of current induced domain wall motion.[84] If a current passes through a magnetic film it gets spin-polarized. If such a current is transferred to a second magnetic layer it can exert a torque on this layer. If the current density is large enough it can change the magnetization of the free electrode. The electrons exert a torque on the magnetization of the upper electrode, whenever the current is applied to the investigated systems. If a critical value is exceeded the magnetization is switched, thus it is possible to change between parallel and antiparallel orientation of the electrodes.

[84] L. Berger, Phys. Rev. B **54** (1996) 9353–9358; L. Berger, J. Appl. Phys. **55(6)** (1984) 1954–1956; L. Berger, J. Appl. Phys. **49** (1978) 2156 –2161; D.C. Ralph and M.D. Stiles, J. Magn. Magn. Mater. **320** (2008) 1190 –1216; J. C. Slonczewski, J. Magn. Magn. Mater. **159** (1996) L1 –L7

For the measurement, the voltage is varied with a triangle envelope function, again with alternating read and write pulses. Figure 36 shows the STT-switching of a single MTJ in a coupled system (cp. Figure 34), which proves that it is possible to switch the elements by current. The graph shows the resistance versus the applied voltage an in comparison the TMR-loop of the same element. The switching from parallel to antiparallel state takes place at a voltage of approximately 700 mVat zero magnetic field. The smaller change for negative voltages is due to the resistive switching with a threshold voltage of approximately 600 mV.

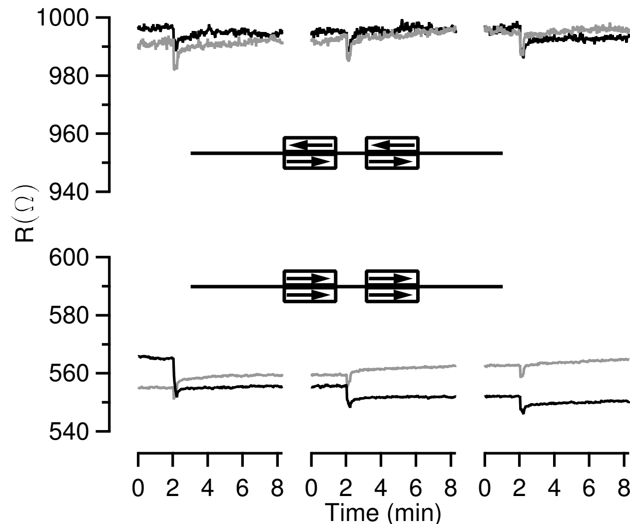

Figure 37: Resistance curves of two head-to-tail coupled MTJs stressed by three consecutive pulse-trains with an amplitude of ±1100 mV. No resistance change can be measured for the antiparallel orientation of the electrodes . The parallel system shows a resistance change of about $\Delta R = 20\,\Omega$.

This is higher than before and can be explained by the higher resistance of the now set antiparallel state of the MTJ.[85] Both curves show the same change of resistance impartial of the way of switching. After showing that it is possible to switch single MTJs into antiparallel state, this can be used in simple coupled systems to raise the net resistance. A much higher critical voltage is necessary to cause the resistive switching, if the elements are in the antiparallel state. Therefore, the actual change in the resistance will go to zero for a completely antiparallel oriented system, as long as the stress voltage is kept constant.

[85] P. Krzysteczko, Dissertation, Universität Bielefeld, 2010

The resistance course of such a double system is shown in Figure 37. Here the two coupled MTJs have a resistance of about $560\,\Omega$ in the parallel and $990\,\Omega$ in the antiparallel orientation of the electrodes. They are stressed by three consecutive pulse-trains for 10 s with a voltage of ± 1100 mV. The completely parallel system shows a resistance change of $\Delta R = 20\,\Omega$, while the antiparallel orientation shows no change at all, as expected.

To sum up, it is possible to switch the magnetization of single

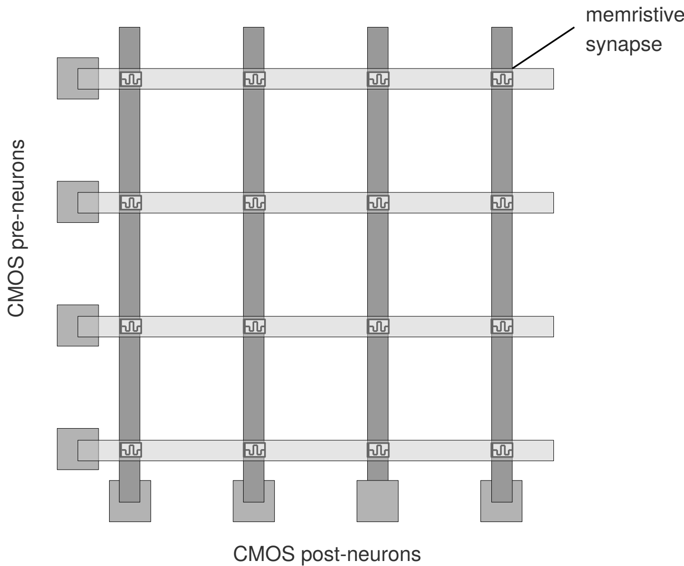

Figure 38: System of memristive synapses combined with CMOS-based pre- and post-neurons in crossbar configuration, based on S. H. Jo et al. , Nano Lett. **10** (2010) 1297–1301.

MTJs in a head-to-tail coupled system with STT-switching, as well as it is possible to enable resistive switching in the parallel orientation of said MTJs and completely suppress it for the antiparallel orientation. This provides an example for a two-component coupled memristive system that can be switched in a either exhibitory or inhibitory state.

The STT-switching of the single MTJs is convenient to manipulate a system of two coupled MTJs but it is inefficient for lager systems, due to the high current densities. The memristive MTJs can likely be optimized to exhibit a memristive effect in the same order of magnitude as the TMR effect, in the future. A possible application can be an array of memristors resembling a biological neuronal network. Such an array would allow to investigate learning behavior and later even features like pattern recognition. A popular design of such an array[86] suggest a neuromorphic system as a hybrid between CMOS and memristor technology. The design of such a system is shown in Figure 38. The crossbar configuration features CMOS-based pre- and postsynaptic neurons an memristive synapse. Such a system would allow to utilize the STDP for learning as well as the usage of the collected data concerning the characteristics of voltage dependence and the influence of the pulse duration on the resistance change in the memristor.

[86] I. Ebong and P. Mazumder, in, Microelectronics (ICM), 2010 International Conference on, 2010, 292 –295; S. H. Jo et al., Nano Lett. **10** (2010) 1297–1301; J.A. Péandrez-Carrasco et al., in, Circuits and Systems (ISCAS), Proceedings of 2010 IEEE International Symposium on, 2010, 1659 –1662

Conclusion

Subject of the presented thesis were two different memristive systems: The first chapter dealt with the development of a memristor based on current induced domain wall motion, the second and third chapter contain the application of memristive MTJs in classic technologies such as MRAM and FPGAs as well as in artificial neural systems.

The cornerstone for a linear memristor was established in the first chapter. It was shown that it is possible to inject domain walls in a structured GMR-system and change the resistance of the stripe current induced. Switching the device between resistance states was achieved with and without applying a bias magnetic field. Micromagnetic simulations were performed to support the conducted measurements, estimating the velocity of the domain wall and accordingly the time scale that is needed for a reliable operation. The simulations were conducted using the OOMMF package from NIST with an add-on for current induced domain wall motion. Based on the simulations it could be shown that current pulses with a duration of 4 ns are needed to control the domain wall position on a length scale of 0.5 μm. At last basic pulse measurements were carried out that proved that a linear memristor is practicable with a proper pulse technique.

The second chapter dealt with the use of memristive MTJs in FPGAs and MRAM to enhance their error tolerance in regard to resistance fluctuation during the fabrication process. The sensitivity concerning the amplitude and duration of the stress pulses was determined to accomplish this. Furthermore, it was shown that it is possible to tune two MTJs with different initial resistance to the same resistance, accordingly raising the error tolerance of FPGAs. This is possible as long as the variances of the resistance in the MTJs are in the same order of magnitude as the memristive effect. In addition, the resistance-state of a stressed MTJ was observed for a duration of 5 h. It appears to be constant for extended periods of time, making refresh cycles to maintain the

resistance-state obsolete. In conclusion, the use of memristive properties in MTJs could be a valuable asset for more reliable, error tolerant spintronics.

The third chapter showed that memristive MTJs exhibit characteristics that closely resemble those of biological synapses, namely LTD and LTP as well as STDP. These properties would allow to create artificial neuronal networks using the memristive MTJs as electronic neurons. Measurements on two coupled memristors were conducted to explore this idea. Whether the resistance change in memristive MTJs is positive or negative depends on the direction of the voltage. The resistance rises for negative voltages and decreases for positive, if the convention of the grounded bottom electrode is minded. This is caused by the localized oxygen vacancies at the interface between bottom electrode and barrier leading to two different ways of connections for a coupled system, back-to-back and head-to-tail. Only the later one was investigated, because in the back-to-back configuration the memristive effects of both elements compete against each other. The result is an equilibrium state dominated by the memristor with the biggest change of resistance. The coupled system showed the memristive effect in the parallel orientation as anticipated. Switching into antiparallel state by keeping the stress voltage constant completely suppresses the resistive switching. As an outlook for the future it is thinkable to create an hybridized artificial neuronal system based on memristive synapses and CMOS neurons that shows STDP. It would be possible to study learning behavior on such a system.

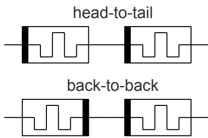

Figure 39: Possible configurations of two memristors.

Appendix

Lithography

The e-beam lithography was performed with a Leo 1530 SEM. The SEM has a 50 m interferometer sample stage from Raith that allows an exact alignment of the sample stage. The negative resist that was used throughout the lithography is the AR-N 7510 from Allresist. The resistance was spincoated to the sample with 6000 rpm for 30 s. To harden the resist it was stored on a heating plate for 2 min at 85^oC. During the lithography the resist is exposed to 300 μAs/cm². The samples are developed in AR 300-47 from Allresist. The etching takes place in an ion-etching machine. An argon plasma is ignited at a low pressure of 10^{-5} mbar. The argon ions etch through the places of the sample that are not covered with the resist. An secondary ion mass spectrometer is connected to the etching machine. The mass spectra allow to stop the etching process in a certain layer. To remove the resist the samples are placed into an ultrasonic-bath with 1-Methyl-2-pyrrolidinone, CHROMASOLV Plus, from Aldrich. The actual lithography differs according to whether a GMR-system or a TMR-system is structured.

Lithography of the GMR system

In Figure 40 the lithography steps of the structured GMR-system are shown. After the application of the resist, the narrow stripes with the domain wall nucleation pad are written in by e-beam. After the developing of the resist the samples are etched down to the substrate. Subsequently the resist is removed in the ultrasonic bath and the sample covered with 6 nm of Ta and 35 nm Au. In the second lithography step the conductive paths are written in the resist. Afterwards the sample is again etched to the substrate and the resist is removed.

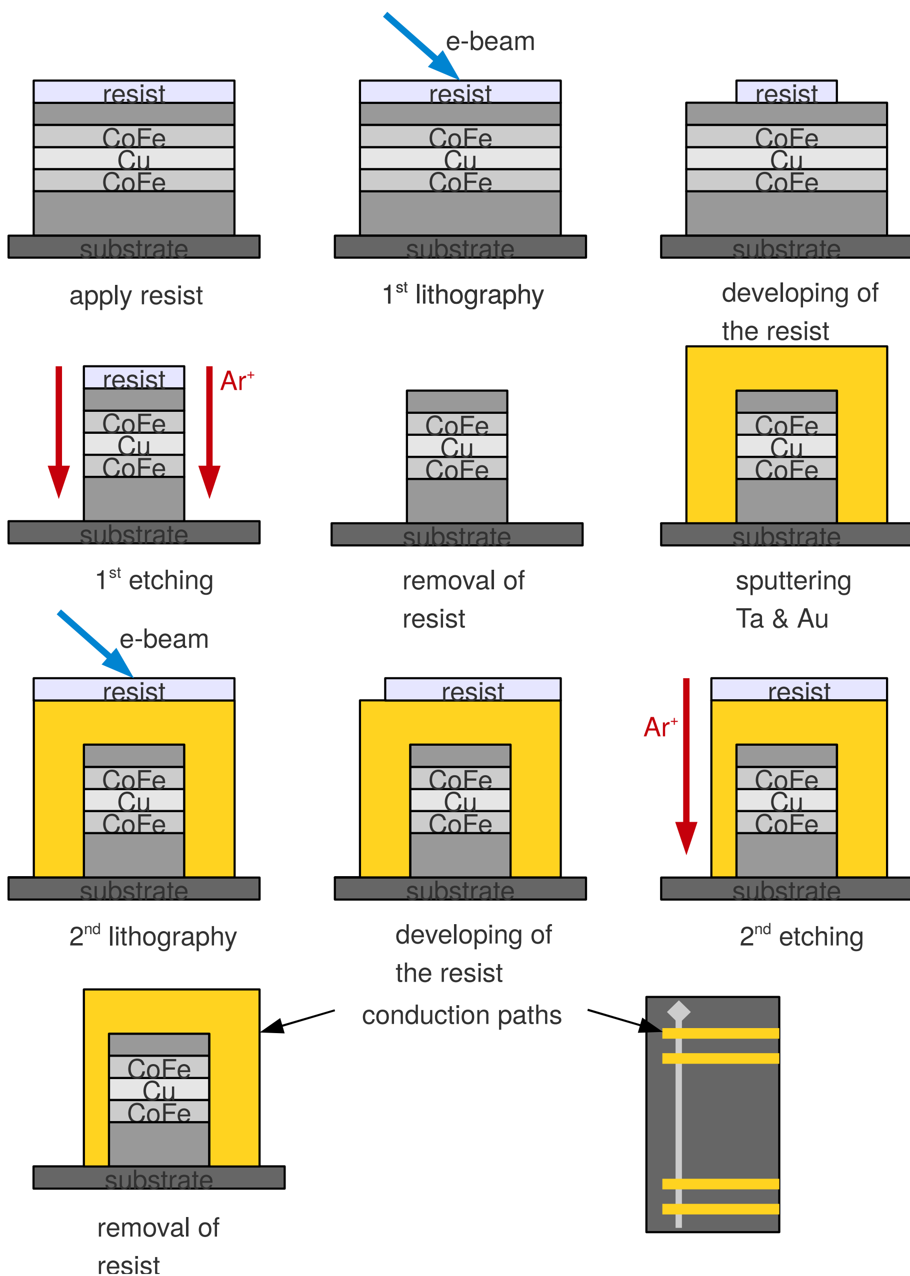

Figure 40: Lithography of the GMR-system

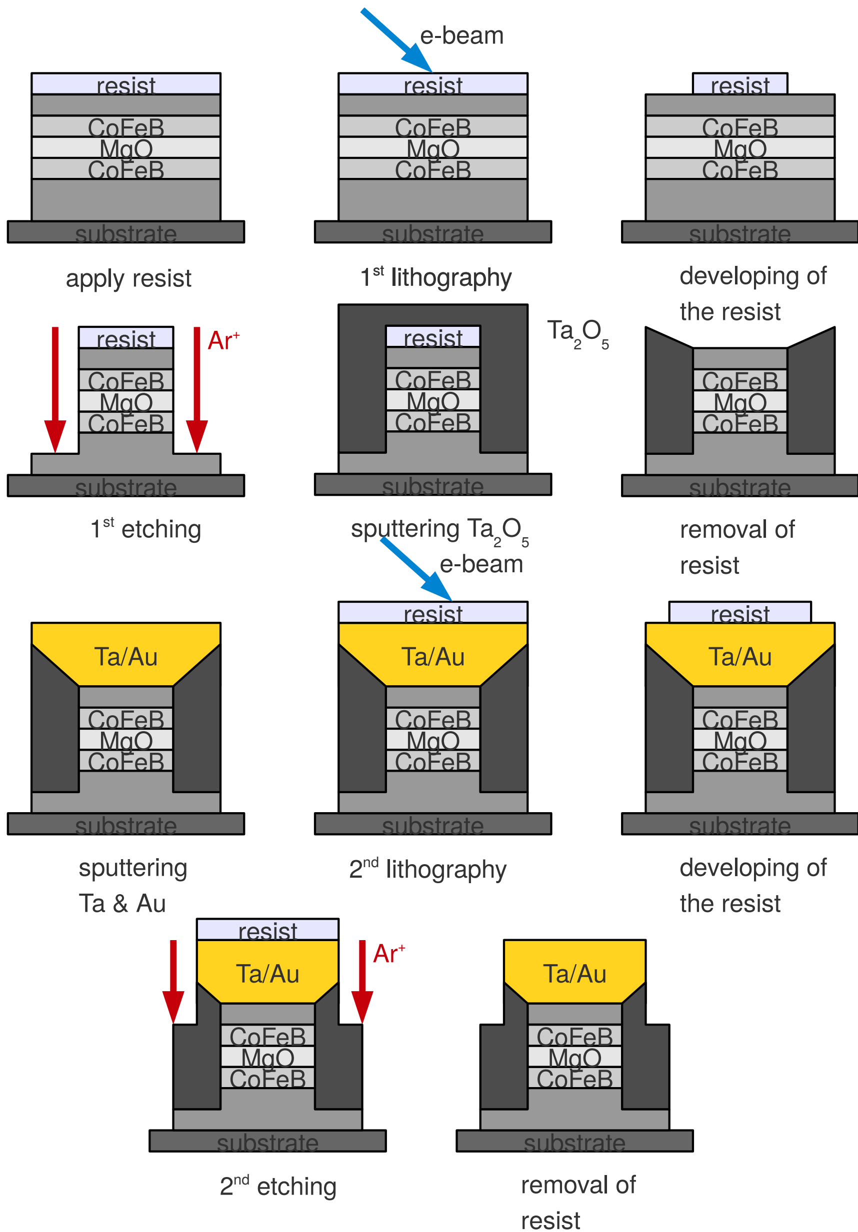

Figure 41: Lithography of the TMR-system

Lithography of the TMR system

Figure 41 shows the steps for the lithography of the MTJs. They are somewhat similar to those of the GMR system. After the application of the resist, ellipses with axes of 300 nm and 150 nm are written in it. After the developing, the samples are etched into elliptical nanopillars. Here, unlike the GMR system, the sample is not etched down to the substrate but the process is stopped after the tunnel-barrier. Subsequently, the pillars are covered with 60 nm insulating Ta_2O_5 with RF-sputter deposition. To remove the resist and the oxide the samples are placed into an ultrasonic bath. Afterwards, Ta and Au are deposited by sputter deposition and the samples are covered with resist. In the second lithography step the contact pads are written in the resist. After developing and etching, the remaining resist is removed in the ultrasonic bath. The Ta_2O_5 is deposited because the structures are to small to contact them without contact pads. If the Ta and Au for the contact pads would be sputtered directly on the nanopillars it would cause a short circuit.

Setup

Measurement of the current induced domain wall motion

Figure 42 depicts the setup for the measurement of the current induced domain wall motion. The sample is measured with the four-point-probe-method with a constant current source. The coils allow to apply an additional external magnetic field to reduced the critical current density.

Measurement of the resistive switching

Figure 43 depicts the setup for the measurement of the resistive switching in the memristive MTJs. Here the sample is characterized by a two-point measurement with a constant voltage source. The coils allow to apply an additional external magnetic field to fix the magnetic orientation of the MTJ.

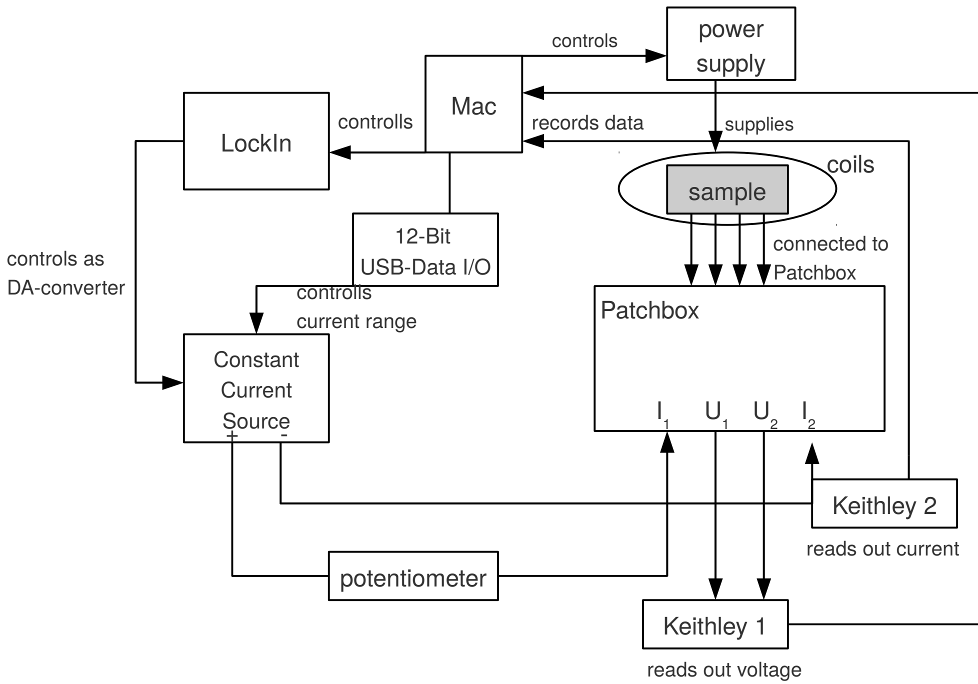

Figure 42: Sketch of the setup for the measurement of current induced domain wall motion.

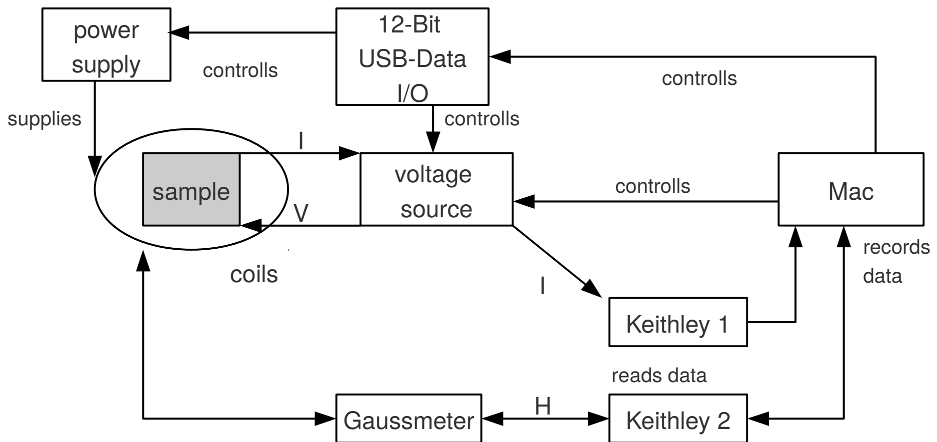

Figure 43: Sketch of the setup for the measurement of resistive switching.

Improved reliability of magnetic field programmable gate arrays through the use of memristive tunnel junctions

Jana Münchenberger,[1,a)] Patryk Krzysteczko,[1] Günter Reiss,[1] and Andy Thomas[1,2]
[1]*Bielefeld University, Thin Films and Physics of Nanostructures, Bielefeld 33615, Germany*
[2]*University of Hamburg, Institute Applied Physics, Hamburg D-20355, Germany*

(Received 6 October 2011; accepted 9 October 2011; published online 10 November 2011)

Since the recent successful implementation of the long-hypothesized memristor, its use in neuronal computing and in the reproduction of biological neural networks has gained increasing attention. In addition to the development of these new applications, the growing number of devices with memristive properties is promising to improve already established technologies. Herein, we use the recently reported memristance in magnesium-oxide-based magnetic tunnel junctions to improve the error tolerance in magnetic random access memory and magnetic field programmable logic arrays. © *2011 American Institute of Physics*. [doi:10.1063/1.3660521]

Magnetic tunnel junctions (MTJs) are electronic devices characterized by two ferromagnetic electrodes separated by a tunnel barrier.[1] MTJs exhibit low- or high-resistance states when the electrodes are in parallel or antiparallel orientations, respectively. This phenomenon is referred to as tunnel magnetoresistance (TMR). These states can be associated with the logical values zero and one.[2] Consequently, when TMR was observed at room temperature,[3,4] the application of MTJs to magnetic random access memory (MRAM),[5] and magnetic field programmable gate arrays (FPGAs),[6] was hypothesized.

However, it has been shown that fluctuations in the resistance of the junctions limit their use in FPGAs. The acceptable level of resistance variation depends on the TMR ratio of the junctions. Distinguishing between high- and low-resistance states is not possible once these variances exceed certain values.[6] Common magnesium-oxide-based MTJs[7,8] exhibit TMR values of up to 600%,[9] though industrially fabricated MRAM and FPGA devices rarely feature TMR ratios above 100%.[10] The recently proposed spin torque MRAM[11–14] requires a thin barrier and low resistance. This results in a TMR ratio of max. 160%,[15,16] for current induced magnetization switching. The variations in the junction resistance are due to either thickness fluctuations in the tunnel barrier or to variability in the junction sizes caused by the lithography process.

Herein, we present data indicating that it is possible to improve the error tolerance of MTJs with memristive[17–20] MgO-based MTJs with thin barriers that exhibit resistive switching.[21–26] The memristance can compensate for the resistance fluctuations and thus improve error tolerance in the next generation of MRAMs and FPGAs.

The memristive MTJs were fabricated via sputter deposition using a Singulus Nano Deposition Timaris tool. The layer stack consisted of (from bottom to top) Ta 3/Cu–N 90/Ta 5/$Pt_{37}Mn_{63}$ 20/$Co_{70}Fe_{30}$ 2/Ru 0.75/$Co_{66}Fe_{22}B_{12}$ 2/MgO 1.3/$Co_{66}Fe_{22}B_{12}$ 3/Ta 10/Cu 30/Ru 7, where the layer thickness is given in nm. The layer stack was annealed at 360 °C in a magnetic field of 1 T. Elliptical pillars are prepared using e-beam lithography and ion beam etching. The ellipses have axes of 150 and 350 nm. A scanning electron microscope (SEM) image of an MTJ is shown in Fig. 1(a).

All transport measurements were performed at room temperature using a constant voltage source and with the bottom electrode grounded. The layer stack exhibits TMR ratios of approximately 100%, as depicted in Fig. 1(b).

During the measurement, a series of alternating read and write pulses were applied as schematically depicted in Fig. 1(c). We initiated the memristive change in resistance using a series of ten write pulses with a length of 1 s each. To determine the resistance, we measured the current during 200-ms read pulses at a readout voltage of 20 mV. To stabilize the magnetic state, a constant magnetic field of 0.04 T was applied during the measurements. All measurements were performed at room temperature.

The resistive switching is similar for junctions from different wafer positions. The memristive effects in the MTJs are assumed to occur because of the displacement of oxygen vacancies.[27] The displacement is believed to occur within a few monolayers at the interface between the MgO barrier. To support this assumption, experiments on postoxidized barriers were performed that showed no memristive effects at all.[28] The interface between the barrier and the electrode is highly sensitive to small changes in its properties. When a voltage exceeding a certain threshold is applied, these vacancies can move in the interface between the MgO barrier and the electrode, which causes a change in the resistance.

This behavior is depicted in Fig. 2. Three pulse trains were applied for every voltage and the resistance change was determined. After completing these measurements, the memristor was reset to its former value with a voltage pulse of the opposite sign. Using the results shown in Fig. 2, it is possible to estimate a threshold voltage of approximately 300 mV. Whenever the applied voltage exceeds this limit, a resistance change can be detected. The inset highlights the changes in resistance from four voltages of −550, −250, +250, and + 550 mV.

The results shown in the graph also indicate that it is possible to target a certain resistance state by applying either

a)Electronic mail: jmuench@physik.uni-bielefeld.de.

 © 2011 American Institute of Physics

Downloaded 09 Feb 2012 to 129.70.54.3. Redistribution subject to AIP license or copyright; see http://jap.aip.org/about/rights_and_permissions

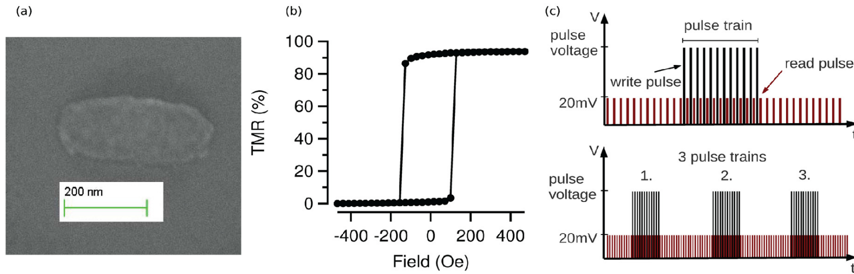

FIG. 1. (Color online) (a) A SEM picture of an MTJ. (b) The minor loop of the MTJ. (c) Measuring technique: A series of alternating read and write pulses were applied to the element. Ten write pulses are called a pulse train. For every investigated voltage, three pulse trains were applied in the following viewgraphs.

a series of pulse trains with smaller amplitudes or a single pulse train with a larger amplitude. This system exhibited a maximum change in resistance of approximately 10 Ω (or 6%). This change is of the same magnitude as the resistance fluctuations observed in the MTJs; in other words, these fluctuations could be counterbalanced using the memristive properties of our MTJs.

We demonstrated this balancing approach through further analyses performed on similar MTJs by tuning two different junctions to the same resistance. These results are presented in Fig. 3, which shows the absolute resistance of the MTJs. As described above, pulse trains with different amplitudes were applied, and the resulting resistances were subsequently measured. These results indicate that it is possible to drive two MTJs with different initial resistances to similar final resistances. We targeted a resistance variation of 1.2% that corresponds to a voltage difference in FPGAs of approximately 450 mV. This is above the threshold for reliable operation of 30 mV.[6]

Furthermore, we confirmed the stability of the memristive change. The resistance level remained stable once it was changed to a specific value, as illustrated in Fig. 4. An MTJ with an initial resistance of approximately 173 Ω was stressed with a voltage pulse of −500 mV to a resistance of 175 Ω. We measured the resistance of the device at a low monitoring voltage, and no change in the resistance could be detected.

In conclusion, we have discussed the potential of memristive MTJs for the optimization of MRAMs and magnetic FPGAs. We have shown that we can tailor the resistances of these devices and thus compensate for resistance fluctuations that occur as a result of the fabrication process. The MTJs maintain stable resistances and do not need to be periodically refreshed. For application in Spin Transfer Torque (STT)-MRAM an additional reset cycle needs to be implemented,

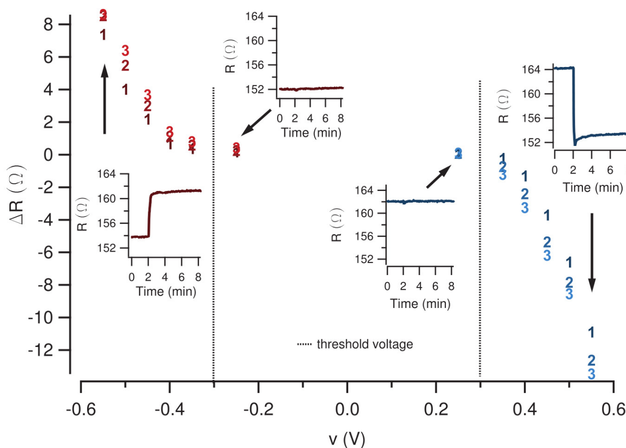

FIG. 2. (Color online) Resistance change as a function of the applied pulse train voltage. Overall, three pulses trains were subsequently applied for every voltage. The resistance value after the first, second, and third pulses train is labeled 1, 2, and 3, respectively. The insets show the change in resistance after applying one pulse. The corresponding data points are marked with arrows. The pulse train was always initiated after 2 min (cf. insets).

Downloaded 09 Feb 2012 to 129.70.54.3. Redistribution subject to AIP license or copyright; see http://jap.aip.org/about/rights_and_permissions

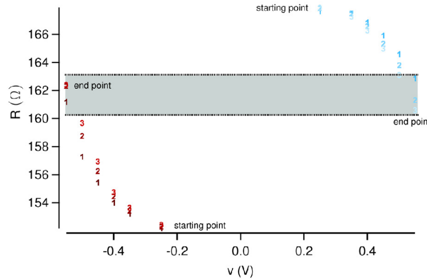

FIG. 3. (Color online) Total resistance of two MTJs with different initial resistances. The left curve and the right curve represent resistance characteristics while stressing the first and the second MTJs with three consecutive pulse trains of variable bias for each datapoint. The gray area represents the resistance target for both MTJs, corresponding to a 1.2% resistance variation.

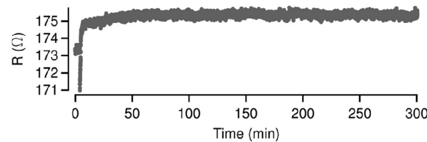

FIG. 4. Long-term measurement of the resistance of an MTJ after stressing with + 500 mV. The element shows no signs of relaxation.

because the high current densities necessary for operation will also trigger the resistive switching.

ACKNOWLEDGMENTS

J.M., P.K., and A.T. acknowledge the financial support from the Ministry of Innovation, Science and Research (MIWF) of North Rhine-Westphalia.

[1] M. Julliere, Phys. Lett. **54A**, 225 (1975).
[2] G. A. Prinz, Science **282**, 1660 (1998).
[3] J. S. Moodera, L. R. Kinder, T. M. Wong, and R. Meservey, Phys. Rev. Lett. **74**, 3273 (1995).
[4] T. Miyazaki and N. Tezuka, J. Magn. Magn. Mater. **139**, L231 (1995).
[5] J. W. C., Black and B. Das, J. Appl. Phys. **87**, 6674 (2000).
[6] G. Reiss and D. Meyners, Appl. Phys. Lett. **88**, 043505 (2006).
[7] S. Yuasa, A. Fukushima, T. Nagahama, K. Ando, and Y. Suzuki, J. Appl. Phys. **43**, L588 (2004).
[8] S. S. P. Parkin, C. Kaiser, A. Panchula, P. M. Rice, B. Hughes, M. Samant, and S.-H. Yang, Nature Mater. **3**, 862 (2004).
[9] S. Ikeda, J. Hayakawa, Y. Ashizawa, Y. M. Lee, K. Miura, H. Hasegawa, M. Tsunoda, F. Matsukura, and H. Ohno, Appl. Phys. Lett. **93**, 082508 (2008).
[10] R. W. Dave, G. Steiner, J. M. Slaughter, J. J. Sun, B. Craigo, S. Pietambaram, K. Smith, G. Grynkewich, M. DeHerrera, J., Åkerman, and S. Tehrani, IEEE Trans. Magn. **42**(8), 1935 (2006).
[11] J. Slonczewski, J. Magn. Magn. Mater. **159**, L1 (1996).
[12] J. A. Katine and E. E. Fullerton, J. Magn. Magn. Mater. **320**, 1217 (2008).
[13] J. Åkerman, Science **308**, 508 (2005).
[14] M. Hosomi, H. Yamagishi, T. Yamamoto, K. Bessho, Y. Higo, K. Yamane, H. Yamada, M. Shoji, H. Hachino, C. Fukumoto, H. Nagao, and H. Kano, in *Electron Devices Meeting, IEDM Technical Digest* (IEEE International, New York, 2005), pp. 459–462.
[15] S. Yuasa, T. Nagahama, A. Fukushima, Y. Suzuki, and K. Ando, Nature Mater. **3**, 868 (2004).
[16] D. H. Lee and S. H. Lim, Appl. Phys. Lett. **92**, 233502 (2008).
[17] L. O. Chua, IEEE Trans. Circuit Theory **CT-18**, 507 (1971).
[18] L. O. Chua and S. Kang, Proc. IEEE **64**, 209 (1976).
[19] D. Strukov, G. S. Snider, D. R. Stewart, and R. S. Williams, Nature **453**, 30 (2008).
[20] M. di Ventra, Y. V. Pershin, and L. O. Chua, Proc. IEEE **97**(8), 1371 (2009).
[21] R. Waser and M. Aono, Nature Mater. **6**, 833 (2007).
[22] M. Janousch, G. I. Meijer, U. Staub, B. Delley, S. F. Karg, and B. P. Andreasson, Adv. Mater. **19**, 2232 (2007).
[23] P. Krzysteczko, X. Kou, K. Rott, A. Thomas, and G. Reiss, J. Magn. Magn. Mater. **321**, 144 (2009).
[24] J. M. Teixeira, J. Ventura, R. Fermento, J. P. Araujo, J. B. Sousa, P. Wisniowski, and P. P. Freitas, J. Phys. D: Appl. Phys. **42**, 105407 (2009).
[25] D. Halley, H. Majjad, M. Bowen, N. Najjari, Y. Henry, C. Ulhaq-Bouillet, W. Weber, G. Bertoni, J. Verbeeck, and G. V. Tendeloo, Appl. Phys. Lett. **92**, 212115 (2008).
[26] C. Yoshida, M. Kurasawa, Y. M. Lee, M. Aoki, and Y. Sugiyama, Appl. Phys. Lett. **92**, 113508 (2008).
[27] J. J. Yang, F. Miao, M. D. Pickett, D. A. A. Ohlberg, D. R. Stewart, C. N. Lau, and R. S. Williams, Nanotechnology **20**, 215201 (2009).
[28] P. Krzysteczko, G. Reiss, and A. Thomas, Appl. Phys. Lett. **95**, 112508 (2009).

Downloaded 09 Feb 2012 to 129.70.54.3. Redistribution subject to AIP license or copyright; see http://jap.aip.org/about/rights_and_permissions

A memristor based on current-induced domain-wall motion in a nanostructured giant magnetoresistance device

Jana Münchenberger,[1,a)] Günter Reiss,[1] and Andy Thomas[1,2]
[1]*Bielefeld University, Thin Films and Physics of Nanostructures, Bielefeld 33615, Germany*
[2]*University of Hamburg, Institute of Applied Physics, Hamburg D-20355, Germany*

(Presented 2 November 2011; received 21 September 2011; accepted 19 October 2011; published online 14 February 2012)

The possibility of controlling the resistance of a memristive giant magnetoresistance (GMR) system via current-induced domain-wall motion was investigated. For a narrow spin-valve structure, current-induced domain-wall motion in the free layer can be detected once the current density exceeds a critical threshold. Then, the resistance of the device depends on the position of the domain wall. The GMR system shows a MR ratio of 10% in the as-prepared state. Narrow stripes were fabricated by e-beam lithography and ion-beam etching with a width of 200 nm. The stripes exhibit GMR ratios up to 8% at room temperature. Micromagnetic simulations of the domain-wall motion in the free layer allow an estimation of the time scale of the domain-wall migration in the stripe. Furthermore, the simulations were compared with measured critical current densities in the free layer with and without an applied external field. © *2012 American Institute of Physics.*
[doi:10.1063/1.3671438]

INTRODUCTION

The memristor as the fourth passive-circuit element has gained a lot of interest in recent years because of its various potential applications, such as new data-storage/processing devices and neuronal computing. Besides the mechanism of resistive switching,[1,2] which is the most well-known implementation of the concepts of a memristor,[3,4] many other systems were suggested, like nanoparticles,[5] or even human blood.[6] An interesting concept was presented theoretically by Wang *et al.*[7,8] using a structured giant magnetoresistance (GMR)[9–11] system and current-induced domain-wall motion to conceptualize a spintronic memristor. In this paper, we investigated the possibility of controlling the resistance of a GMR system by current-induced domain-wall motion. If the lateral size of a magnetic layer is constricted, a transition from multidomain states to single domain states takes place. For such a narrow structure, current-induced domain-wall motion is predicted as soon as the current density reaches a critical threshold.[12–14] The investigated GMR systems exhibit two resistance states, depending on their magnetic orientation. We refer to them as high-resistance state (HRS) and low-resistance state (LRS). As in simple magnetic layers, a transition to single domain states is expected, as well as current-induced domain-wall motion.[15] The resistance of such a structured GMR system depends solely on the position of the domain wall in the free layer, as shown in Fig. 1(a). The resistance per unit length is defined through the relative magnetic orientation of the free layer compared to the reference layer. For parallel orientation, we observe a low resistance and for antiparallel orientation, a high resistance. The resistance of the device then becomes: $R = r_H \cdot x + r_L \cdot (D - x)$, with r_H and r_L as resistance per unit length in the parallel and antiparallel case, respectively, D as length of the structure, and x as position of the domain wall within the structure.[7,8] Therefore, it should be possible to move the domain wall continuously through the structure and get a linear progression of the resistance. The result would be a linear spintronic memristor.

The GMR-layer stack was provided by Infineon, Regensburg (Germany) and had the following layer sequence: (bottom) Si/Ta 3/Py 2/PtMn 15/CoFe 2/Ru 1/CoFe 2/Cu 2/CoFe 5/TaN 10 (top). The layer thicknesses are given in nanometers. In the as-prepared state, around 10% GMR ratio can be measured. The samples are structured with e-beam lithography and ion-beam etching. The structure consists of a domain-wall nucleation pad (DWNP) and a 200-nm-wide stripe. On this structure, four contacts are written in a second lithography step. The samples are measured with a four-point-method with a constant current source. To determine the critical current density, the applied current is varied and the resistance of the device is measured. An optional magnetic field can be applied to reduce the critical current density. All measurements were performed at room temperature. Figure 1 shows the design of the DWNP and a typical GMR minor loop of a structured element with 8% GMR ratio. The slightly diminished GMR ratio may occur because of edge effects in the structured layers. The samples show a sharp switching behavior, without steps, which suggests few pinning centers for the domain wall within the structure. We performed measurements to determine the critical current density. To support the current-induced domain-wall motion, bias magnetic fields of +59 Oe and −45 Oe were applied for the two directions of domain-wall motion, respectively. Those fields are near the switching fields of the GMR device. Figure 2 shows two consecutive measurements with different bias fields. A distinct switching in the HRS and LRS is discernible at certain current densities. Also, we assert that the resistance states are stable

a)Electronic mail: jmuench@physik.uni-bielefeld.de.

 © 2012 American Institute of Physics

Downloaded 14 Feb 2012 to 129.70.54.3. Redistribution subject to AIP license or copyright; see http://jap.aip.org/about/rights_and_permissions

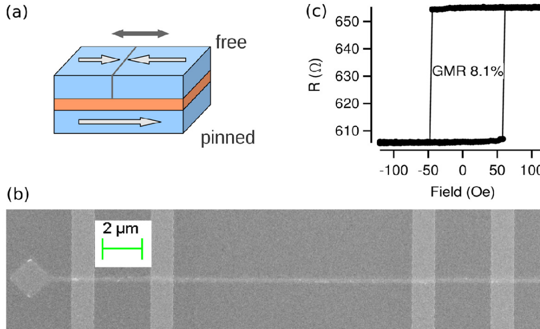

FIG. 1. (Color online) (a) Sketch of the idea of a memristor based on current-induced domain-wall motion. The resistance of the device depends solely on the position of the domain wall. (b) SEM image of the structure with a domain-wall nucleation pad. In (c), a GMR curve of a structured device is pictured. The samples exhibit a GMR ratio of about 8%.

until further interaction with the system. The distortion of the resistance curve besides the sharp switching occurs because of Joule heating of the sample for high currents. The critical current densities of $1.9 \cdot 10^{11}$ A/m^2 and $1.2 \cdot 10^{11}$ A/m^2 match those of similar systems.[16] In Fig. 2(b), the *IV* curve is presented. The ends of the curve show a splitting (marked with arrows in the graph). This splitting is characteristic for memristive systems. Whereas the overall change in the resistance can be measured, the conducted experiment does not allow estimating the velocity of a domain wall moving through the stripe. For this purpose, micromagnetic simulation was performed. We used the object-oriented micromagnetic framework (OOMMF) from NIST to simulate the system. An add-on for OOMMF to simulate current-induced domain-wall motion was developed by IBM Zürich.[17–19] To calculate the motion of the domain wall, the program solves the Landau-Lifshitz-Gilbert equation with a spin-torque term along the wire:

$$\dot{\mathbf{m}} = -|\gamma|\mathbf{H}_{\text{eff}} \times \mathbf{m} + \alpha\mathbf{m} \times \dot{\mathbf{m}} + u \cdot \mathbf{m} \times \left(\mathbf{m} \times \frac{\partial \mathbf{m}}{\partial x}\right) + \beta \cdot u \cdot \mathbf{m} \times \frac{\partial \mathbf{m}}{\partial x},$$

with α and β as dimensionless parameters concerning phenomenological damping, whereas $\mathbf{m}$ is the unit vector of the magnetization, γ the gyromagnetic ratio, and $\mathbf{H}_{\text{eff}}$ the effective field. u can be identified as a velocity equivalent:

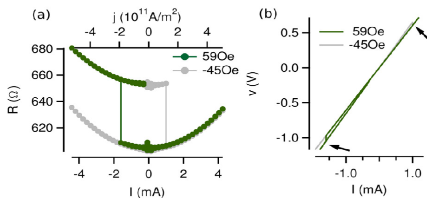

FIG. 2. (Color online) (a) Resistance vs current and current density measured at applied bias fields. The warping in the curve is because of Joule heating. The critical current densities are reached at $1.9 \cdot 10^{11}$ A/m^2 for a bias field of -45 Oe and $1.2 \cdot 10^{11}$ A/m^2 for 59 Oe. (b) *IV* curve of the device. The curve shows a splitting characteristic for memristive systems at the end.

$$u = \frac{\text{JgP}\mu_{\text{B}}}{2\text{eM}_{\text{S}}}.$$

Herein J is the current density, g the Landé factor, P the current polarization, μ_B the Bohr magnetron, e the elementary charge, and M_S the saturation magnetization. To simplify the problem, only the domain-wall motion of the CoFe free layer is considered. The simulated device has dimensions of 5 nm $\times$ 200 nm $\times$ 5000 nm. First, the applied magnetic field is set to 50 Oe. We choose for J the measured current density of $1.2 \cdot 10^{11}$ A/m^2, a current polarization of 0.8, and a M_S of $1300 \cdot 10^3$ A/m.[20,21] As an additional parameter, the program is given an exchange constant A of $3 \cdot 10^{12}$ J/m. α, the Gilbert damping constant, and β constant non-adiabaticity parameters are set to 0.005 and 0.04, respectively. We can calculate a velocity of 100 m/s. To check the calculations, we performed simulations at zero field determining the critical current density necessary for domain-wall motion. In Fig. 3(a), the motion of the domain wall through the stripe at zero field is shown. The simulated current density is $5.6 \cdot 10^{11}$ A/m^2 and the mean velocity is approximately 125 m/s. The resistance and the domain-wall displacement depending on the time for the simulated stripe are presented in Fig. 3. After a phase of acceleration of the domain wall, the resistance change is approximately linear. For HRS and LRS, the resistance change of the sample in Fig. 3(c) was used. Here, a measurement on a structured GMR system at zero field exhibits a switching at around $5.72 \cdot 10^{11}$ A/m^2. This matches the simulation considering that a real wire most likely features imperfections that act as pinning centers for domain walls because of the lithography process.

We show that it is possible to build a linear memristor based on current-induced domain-wall motion in a structured GMR system. This prototype could be driven between HRS and LRS even without an applied magnetic field. The splitting in the *IV* curve shows a general memristive characteristic. We performed simulations to determine the time scale of the domain-wall motion. To control the domain-wall position on a length scale of 0.5 μm, the time resolution has to be below 4 ns for the zero-field measurements. In recent publications,[22,23] detailed control over domain walls was shown using pulses of nanosecond length to control the

Downloaded 14 Feb 2012 to 129.70.54.3. Redistribution subject to AIP license or copyright; see http://jap.aip.org/about/rights_and_permissions

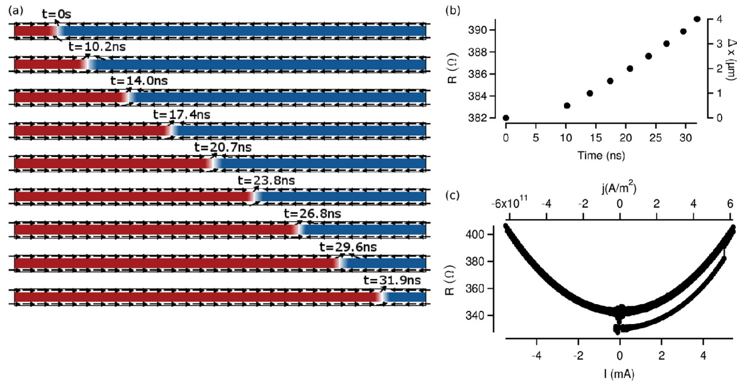

FIG. 3. (Color online) (a) Simulated motion of the domain wall along the wire at zero field and a current density of $5.6 \cdot 10^{11}$ A/m^2. (b) Calculated resistance depending on domain-wall displacement and time. (c) Measured switching curve on a device at zero field at a current density of $5.72 \cdot 10^{11}$ A/m^2. The HRS and LRS were used to calculate the steps in (b).

domain-wall position. The application of pulse techniques thus would allow tuning the resistance between HRS and LRS and vice versa; because the direction of the resistance change depends reproducibly on the current pulse direction, this behavior corresponds to a linear memristor. Additionally, the GMR-based memristor can be used as a robust and fast device for application, e.g., in artificial neural networks to mimic systems of neurocytes, or as a sensor.

ACKNOWLEDGMENTS

A.T. and J.M. acknowledge the MIWF of the NRW state government for financial support. J.M. and G.R. acknowledge funding from the DFG Grant Re 1052/20-1.

[1]D. Strukov, G. S. Snider, D. R. Stewart, and R. S. Williams, Nature **453**, 30 (2008).
[2]P. Krzysteczko, G. Reiss, and A. Thomas, Appl. Phys. Lett. **95**, 112508 (2009).
[3]L. O. Chua, IEEE Trans. Circuit Theory **CT-18**, 507 (1971).
[4]L. O. Chua and S. M. Kang, Proc. IEEE **64**, 209 (1976).
[5]T. H. Kim, E. Y. Jang, N. J. Lee, D. J. Choi, K.-J. Lee, J.-T. Jang, J.-S. Choi, S. H. Moon, and J. Cheon, Nano Lett. **9**, 2229 (2009).
[6]S. Kosta, Y. Kosta, M. Bhatele, Y. Dubey, A. Gaur, S. Kosta, J. Gupta, A. Patel, and B. Patel, Int. J. Med. Eng. Inf. **3**, 16 (2011).
[7]X. Wang, Y. Chen, H. Xi, H. Li, and D. Dimitrov, IEEE Electron Device Lett. **30**, 294 (2009).
[8]Y. Chen and X. Wang, in *Symposium on Nanoscale Architectures, 2009. NANOARCH'09. IEEE/ACM International* (IEEE, New York, 2009), pp. 7–12.
[9]P. Grünberg, R. Schreiber, Y. Pang, M. B. Brodsky, and H. Sowers, Phys. Rev. Lett. **57**, 2442 (1986).
[10]M. N. Baibich, J. M. Broto, A. Fert, F. N. Van Dau, F. Petroff, P. Etienne, G. Creuzet, A. Friederich, and J. Chazelas, Phys. Rev. Lett. **61**, 2472 (1988).
[11]G. Binasch, P. Grünberg, F. Saurenbach, and W. Zinn, Phys. Rev. B **39**, 4828 (1989).
[12]L. Berger, J. Appl. Phys. **55**(6), 1954 (1984).
[13]L. Berger, Phys. Rev. B **54**, 9353 (1996).
[14]J. C. Slonczewski, J. Magn. Magn. Mater. **159**, L1 (1996).
[15]J. Grollier, P. Boulenc, V. Cros, A. Hamzic, A. Vaures, A. Fert, and G. Faini, Appl. Phys. Lett. **83**, 509 (2003).
[16]Y. Jang, S. Yoon, K. Lee, S. Lee, C. Nam, and B. K. Cho, Nanotechnology **20**, 125401.
[17]S. Zhang and Z. Li, Phys. Rev. Lett. **93**, 127204 (2004).
[18]A. Thiaville, Y. Nakatani, J. Miltat, and Y. Suzuki, Europhys. Lett. **69**, 990 (2005).
[19]A. Vanhaverbeke and M. Viret, Phys. Rev. B **75**, 024411 (2007).
[20]Y. Ren, H. Zhao, Z. Zhang, and Q. Y. Jin, Appl. Phys. Lett. **92**, 162513 (2008).
[21]P. M. Braganca, B. A. Gurney, B. A. Wilson, J. A. Katine, S. Maat, and J. R. Childress, Nanotechnology **21**, 235202 (2010).
[22]X. Jiang, L. Thomas, R. Moriya, and S. S. P. Parkin, Nano Lett. **11**, 96 (2011).
[23]L. Heyne, J. Rhensius, A. Bisig, S. Krzyk, P. Punke, M. Kläui, L. J. Heyderman, L. L. Guyader, and F. Nolting, Appl. Phys. Lett. **96**, 032504 (2010).

Downloaded 14 Feb 2012 to 129.70.54.3. Redistribution subject to AIP license or copyright; see http://jap.aip.org/about/rights_and_permissions

Bibliography

[1] J. Åkerman, *Toward a Universal Memory*, Science **308** (2005) 508–510, DOI: 10.1126/science.1110549.

[2] R. Ananthanarayanan et al., "The cat is out of the bag: cortical simulations with 10^9 neurons, 10^{13} synapses", in, Proceedings of the Conference on High Performance Computing Networking, Storage and Analysis, SC '09, Portland, Oregon: ACM, 2009, 63:1–63:12, DOI: http://doi.acm.org/10.1145/1654059.1654124.

[3] M. N. Baibich et al., *Giant Magnetoresistance of (001)Fe/(001)Cr Magnetic Superlattices*, Phys. Rev. Lett. **61** (1988) 2472–2475, DOI: 10.1103/PhysRevLett.61.2472.

[4] G.S.D. Beach, M. Tsoi and J.L. Erskine, *Current-induced domain wall motion*, J. Magn. Magn. Mater. **320** (2008) 1272 –1281, DOI: 10.1016/j.jmmm.2007.12.021.

[5] C. C. Bell et al., *Synaptic plasticity in a cerebellum-like structure depends on temporal order*, Nature **387** (1997) 278 –281, DOI: 10.1038/387278a0.

[6] L. Berger, *Emission of spin waves by a magnetic multilayer traversed by a current*, Phys. Rev. B **54** (1996) 9353–9358, DOI: 10.1103/PhysRevB.54.9353.

[7] L. Berger, *Exchange interaction between ferromagnetic domain wall and electric current in very thin film*, J. Appl. Phys. **55(6)** (1984) 1954–1956, DOI: 10.1063/1.333530.

[8] L. Berger, *Low-field magnetoresistance and domain drag in ferromagnets*, J. Appl. Phys. **49** (1978) 2156 –2161, DOI: 10.1063/1.324716.

[9] B. Berninger and G.-Q. Bi, *Synaptic modification in neural circuits: A timely action*, BioEssays **24** (2002) 212–222, DOI: 10.1002/bies.10060.

[10] G. Bi and M. Poo, *Synaptic Modifications in Cultured Hippocampal Neurons: Dependence on Spike Timing, Synaptic Strength, and Postsynaptic Cell Type*, J. Neurosci. **18** (1998) 10464–10472.

[11] G. Binasch et al., *Enhanced magnetoresistance in layered magnetic structures with antiferromagnetic interlayer exchange*, Phys. Rev. B **39** (1989) 4828–4830, DOI: 10.1103/PhysRevB.39.4828.

[12] J. Borghetti et al., *'Memristive' switches enable 'stateful' logic operations via material implication*, Nature **464** (2010) 873–876, DOI: 10.1038/nature08940.

[13] P. M. Braganca et al., *Nanoscale magnetic field detection using a spin torque oscillator*, Nanotech. **21** (2010) 235202, DOI: 10.1088/0957-4484/21/23/235202.

[14] W. H. Butler et al., *Spin-dependent tunneling conductance of Fe | MgO | Fe sandwiches*, Phys. Rev. B **63** (2001) 054416, DOI: 10.1103/PhysRevB.63.054416.

[15] Campbell, *Biology*, Peason Education, 2011.

[16] Y. Chen and X. Wang, "Compact modeling and corner analysis of spintronic memristor", in, IEEE/ACM International Symposium on Nanoscale Architectures, 2009. NANOARCH '09., 2009, 7 –12, DOI: 10.1109/NANOARCH.2009.5226363.

[17] L. O. Chua, *Memristor-The Missing Circuit Element*, IEEE Transactions on circuit theory **CT-18** (1971) 507–519, DOI: 10.1109/TCT.1971.1083337.

[18] L. O. Chua and Sung Mo Kang, *Memristive devices and systems*, Proceedings of the IEEE **64** (1976) 209–223, DOI: 10.1109/PROC.1976.10092.

[19] M. T. Dang et al., *Disrupted motor learning and long-term synaptic plasticity in mice lacking NMDAR1 in the striatum*, PNAS **103** (2006) 15254–15259, DOI: 10.1073/pnas.0601758103.

[20] R.W. Dave et al., *MgO-Based Tunnel Junction Material for High-Speed Toggle Magnetic Random Access Memory*, Magnetics, IEEE Transactions on **42** (2006) 1935 –1939, DOI: 10.1109/TMAG.2006.877743.

[21] M.J. Donahue and D.G. Porter, *OOMMF User's Guide, Version 1.0*, Interagency Report **NISTIR 6376** (1999) National Institute of Standards and Technology, Gaithersburg, MD, URL: `http://math.nist.gov/oommf`.

[22] I. Ebong and P. Mazumder, "Memristor based STDP learning network for position detection", in, Microelectronics (ICM), 2010 International Conference on, 2010, 292 –295, DOI: `10.1109/ICM.2010.5696142`.

[23] A. Elshabini-Riad and F. D. Barlow III, *Thin Film Technology Handbook*, McGraw Hill, 1998.

[24] T. L. Gilbert, Physical Review **100** (1955) 1243.

[25] T.L. Gilbert, *A phenomenological theory of damping in ferromagnetic materials*, Magnetics, IEEE Transactions on **40** (2004) 3443 –3449, DOI: `10.1109/TMAG.2004.836740`.

[26] J. Grollier et al., *Switching a spin valve back and forth by current-induced domain wall motion*, Appl. Phys. Lett. **83** (2003) 509–511, DOI: `10.1063/1.1594841`.

[27] P. Grünberg et al., *Layered Magnetic Structures: Evidence for Antiferromagnetic Coupling of Fe Layers across Cr Interlayers*, Phys. Rev. Lett. **57** (1986) 2442–2445, DOI: `10.1103/PhysRevLett.57.2442`.

[28] J. S. Haas, B. Zavala and C. E. Landisman, *Activity-Dependent Long-Term Depression of Electrical Synapses*, Science **334** (2011) 389–393, DOI: `10.1126/science.1207502`.

[29] D. Halley et al., *Electrical switching in Fe/Cr/MgO/Fe magnetic tunnel junctions*, Appl. Phys. Lett. **92** (2008) 212115, DOI: `10.1063/1.2938696`.

[30] U. Hartmann et al., *Magnetic Multilayers and Giant Magnetoresistance*, Springer, 1999.

[31] B. Hausmanns, *Magnetowiderstand und Ummagnetisierungsprozesse in einzelnen nanostrukturierten magnetischen Leiterbahnen*, Dissertation, Universität Essen/Duisburg, 2003.

[32] D. O. Hebb, *The organization of behaviour*, 1949.

[33] L. Heyne et al., *Direct observation of high velocity current induced domain wall motion*, Appl. Phys. Lett. **96** (2010) 032504, DOI: `10.1063/1.3291067`.

[34] A. L. Hodgkin and A. F. Huxley, *A quantitative description of membrane current and its application to conduction and excitation in nerve*, J. Physiol. **117** (1952) 500–544.

[35] M. Hosomi et al., "A novel nonvolatile memory with spin torque transfer magnetization switching: spin-ram", in, Electron Devices Meeting, 2005. IEDM Technical Digest. IEEE International, 2005, 459 –462, DOI: 10.1109/IEDM.2005.1609379.

[36] Y. Huai et al., *Spin-transfer switching in MgO magnetic tunnel junction nanostructures*, J. Magn. Magn. Mater. **304** (2006) 88 –92, DOI: 10.1016/j.jmmm.2006.04.016.

[37] S. Ikeda et al., *Tunnel magnetoresistance of 604% at 300 K by suppression of Ta diffusion in CoFeB/MgO/CoFeB pseudo-spin-valves annealed at high temperature*, Appl. Phys. Lett. **93** (2008) 082508, DOI: 10.1063/1.2976435.

[38] Y. Jang et al., *Current-induced domain wall nucleation and its pinning characteristics at a notch in a spin-valve nanowire*, Nanotech. **20** 125401, DOI: 10.1088/0957-4484/20/12/125401.

[39] M. Janousch et al., *Role of Oxygen Vacancies in Cr-Doped SrTiO3 for Resistance-Change Memory*, Adv. Mater. **19** (2007) 2232–2235, DOI: 10.1002/adma.200602915.

[40] X. Jiang et al., *Discrete Domain Wall Positioning Due to Pinning in Current Driven Motion along Nanowires*, Nano Lett. **11** (2011) 96–100, DOI: 10.1021/nl102890h.

[41] S. H. Jo et al., *Nanoscale Memristor Device as Synapse in Neuromorphic Systems*, Nano Lett. **10** (2010) 1297–1301, DOI: 10.1021/nl904092h.

[42] M. Julliere, *Tunneling between ferromagnetic films*, Phys. Lett. **54 A** (1975) 225–226, DOI: 10.1016/0375-9601(75)90174-7.

[43] J.A. Katine and Eric E. Fullerton, *Device implications of spin-transfer torques*, J. Magn. Magn. Mater. **320** (2008) 1217 – 1226, DOI: 10.1016/j.jmmm.2007.12.013.

[44] T. H. Kim et al., *Nanoparticle assemblies as memristors*, Nano Lett. **9** (2009) 2229–2233, DOI: 10.1021/nl101926w.

[45] S. P. Kosta et al., *Human blood liquid memristor*, International Journal of Medical Engineering and Informatics **3** (2011) 16 –29, DOI: 10.1504/IJMEI.2011.039073.

[46] P. Krzysteczko, *Memristive tunnel junctions*, Dissertation, Universität Bielefeld, 2010.

[47] P. Krzysteczko, G. Reiss and A. Thomas, *Memristive switching of MgO based magnetic tunnel junctions*, Appl. Phys. Lett. **95** 112508(2009) 112508, DOI: 10.1063/1.3224193.

[48] P. Krzysteczko et al., *Current induced resistance change of magnetic tunnel junctions with ultra-thin MgO tunnel barriers*, J. Magn. and Magn. Mater. **321** (2009) 144 –147, DOI: 10.1016/j.jmmm.2008.08.088.

[49] P. Krzysteczko et al., *The Memristive Magnetic Tunnel Junction as a Nanoscopic Synapse-Neuron System*, Adv. Mater. (2012) 762–766, DOI: 10.1002/adma.201103723.

[50] H. Kuchling, *Taschenbuch der Physik*, Fachbuchverlag Leipzig im Carl Hanser Verlag, 2011.

[51] L. D. Landau and E. M. Lifshitz, Phys. Z. Sowjet. **8** (1935) 153 –169.

[52] D. H. Lee and S. H. Lim, *Increase of temperature due to Joule heating during current-induced magnetization switching of an MgO-based magnetic tunnel junction*, Appl. Phys. Lett. **92** (2008) 233502, DOI: 10.1063/1.2943151.

[53] J. C. Magee and D. Johnston, *A Synaptically Controlled, Associative Signal for Hebbian Plasticity in Hippocampal Neurons*, Science **275** (1997) 209–213, DOI: 10.1126/science.275.5297.209.

[54] H. Markram et al., *Regulation of Synaptic Efficacy by Coincidence of Postsynaptic APs and EPSPs*, Science **275** (1997) 213–215, DOI: 10.1126/science.275.5297.213.

[55] J. Mathon and A. Umerski, *Theory of tunneling magnetoresistance of an epitaxial Fe/MgO/Fe(001) junction*, Phys. Rev. B **63** (2001) 220403, DOI: 10.1103/PhysRevB.63.220403.

[56] D. Meyners et al., *Submicron-sized magnetic tunnel junctions in field programmable logic gate arrays*, J. Appl. Phys. **99** 023907, DOI: 10.1063/1.2164540.

[57] T. Miyazaki and N. Tezuka, *Giant magnetic tunneling effect in Fe/Al2O3/Fe junction*, J. Magn. Magn. Mater. **139** (1995) L231 –L2340, DOI: DOI:10.1016/0304-8853(95)90001-20.

[58] J. S. Moodera et al., *Large Magnetoresistance at Room Temperature in Ferromagnetic Thin Film Tunnel Junctions*, Phys. Rev. Lett. **74** (1995) 3273–3276, DOI: 10.1103/PhysRevLett.74.3273.

[59] N. F. Mott, *The Electrical Conductivity of Transition Metals*, Proc. R. Soc. Lond. **A 153** (1936) 699–717, DOI: 10.1098/rspa.1936.0031.

[60] J. Münchenberger, G. Reiss and A. Thomas, *A memristor based on current-induced domain-wall motion in a nanostructured giant magnetoresistance device*, J. Appl. Phys. **111** (2012) 07D303, DOI: 10.1063/1.3671438.

[61] J. Münchenberger et al., *Improved reliability of magnetic field programmable gate arrays through the use of memristive tunnel junctions*, J. Appl. Phys. **110** (2011) 096105 –096105, DOI: 10.1063/1.3660521.

[62] J. Nogués and I. K. Schuller, *Exchange bias*, J. Magn. Magn. Mater. **192** (1999) 203 –232, DOI: 10.1016/S0304-8853(98)00266-2.

[63] S. S. P. Parkin et al., *Giant tunnelling magnetoresistance at room temperature with MgO (100) tunnel barriers*, Nature Mater. **3** (2004) 862 –867, DOI: 10.1038/nmat1256.

[64] J.A. Pé andrez-Carrasco et al., "On neuromorphic spiking architectures for asynchronous STDP memristive systems", in, Circuits and Systems (ISCAS), Proceedings of 2010 IEEE International Symposium on, 2010, 1659 –1662, DOI: 10.1109/ISCAS.2010.5537484.

[65] Y. V. Pershin, S. La Fontaine and M. Di Ventra, *Memristive model of amoeba learning*, Phys. Rev. E **80** (2009) 021926, DOI: 10.1103/PhysRevE.80.021926.

[66] G. A. Prinz, *Magnetoelectronics*, Science **282** (1998) 1660–1663, DOI: 10.1126/science.282.5394.1660.

[67] D.C. Ralph and M.D. Stiles, *Spin transfer torques*, J. Magn. Magn. Mater. **320** (2008) 1190 –1216, DOI: 10.1016/j.jmmm.2007.12.019.

[68] G. Reiss and D. Meyners, *Reliability of field programmable magnetic logic gate arrays*, Appl. Phys. Lett. **88** (2006) 043505, DOI: 10.1063/1.2167609.

[69] Y. Ren et al., *Ultrafast optical modulation of exchange coupling in FePt/CoFe composite structure*, Appl. Phys. Lett. **92** (2008) 162513, DOI: 10.1063/1.2916704.

[70] R. Richter et al., *Nonvolatile field programmable spin-logic for reconfigurable computing*, Appl. Phys. Lett. **80** (2002) 1291–1293, DOI: 10.1063/1.1449536.

[71] K. Seo et al., *Analog memory and spike-timing-dependent plasticity characteristics of a nanoscale titanium oxide bilayer resistive switching device*, Nanotech. **22** (2011) 254023, DOI: 10.1088/0957-4484/22/25/254023.

[72] J. C. Slonczewski, *Current-driven excitation of magnetic multilayers*, J. Magn. Magn. Mater. **159** (1996) L1 –L7, DOI: 10.1016/0304-8853(96)00062-5.

[73] G. S. Snider, *Self-organized computation with unreliable, memristive nanodevices*, Nanotech. **18** (2007) 365202, DOI: 10.1088/0957-4484/18/36/365202.

[74] S. Song, K. D. Miller and L. F. Abbott, *Competitive Hebbian learning through spike-timing-dependent synaptic plasticity*, Nature Neurosci. **3** (2000) 919 –926, DOI: 10.1038/78829.

[75] D.B. Strukov et al., *The missing memristor found*, Nature **453** (2008) 30–83, DOI: 10.1038/nature06932.

[76] P. M. Tedrow and R. Meservey, *Spin-Dependent Tunneling into Ferromagnetic Nickel*, Phys. Rev. Lett. **26** (1971) 192–195, DOI: 10.1103/PhysRevLett.26.192.

[77] J. M. Teixeira et al., *Electroforming, magnetic and resistive switching in MgO-based tunnel junctions*, J. Phys. D: Appl. Phys. **42** (2009) 105407, DOI: 10.1088/0022-3727/42/10/105407.

[78] A. Thiaville et al., *Micromagnetic understanding of current-driven domain wall motion in patterned nanowires*, Europhys. Lett. **69** (2005) 990, DOI: 10.1209/epl/i2004-10452-6.

[79] T. P. Trappenberg, *Fundamentals of Computational Neuroscience*, Oxford University Press, 2010.

[80] A. Vanhaverbeke and M. Viret, *Simple model of current-induced spin torque in domain walls*, Phys. Rev. B **75** (2007) 024411, DOI: 10.1103/PhysRevB.75.024411.

[81] J. A. Venables, *Introduction to Surface and Thin film Processes*, Cambridge University Press, 2000.

[82] X. Wang et al., *Spintronic Memristor Through Spin-Torque-Induced Magnetization Motion*, Electron Device Letters, IEEE **30** (2009) 294 –297, DOI: 10.1109/LED.2008.2012270.

[83] K. Wasa and S. Hayakawa, *Handbook of sputter deposition technology*, Noyes Publications, 1992.

[84] R. Waser and M. Aono, *Nanoionics-based resistive switching memories*, Nature Mater. **6** (2007) 833 –840, DOI: 10.1038/nmat2023.

[85] Jr. W. C. Black and B. Das, *Programmable logic using giant-magnetoresistance and spin-dependent tunneling devices (invited)*, J. Appl. Phys. **87** (2000) 6674–6679, DOI: 10.1063/1.372806.

[86] B. Widrow, Stanford Electronics Laboratories Technical Report **1553** (1960)

[87] C. Yoshida et al., *Unipolar resistive switching in CoFeB/MgO/CoFeB magnetic tunnel junction*, Appl. Phys. Lett. **92** (2008) 113508, DOI: 10.1063/1.2898514.

[88] S. Yuasa and D. D. Djayaprawira, *Giant tunnel magnetoresistance in magnetic tunnel junctions with a crystalline MgO(0 0 1) barrier*, J. Phys. D: Appl. Phys. **40** (2007) R337, DOI: 10.1088/0022-3727/40/21/R01.

[89] S. Yuasa et al., *Giant room-temperature magnetoresistance in single-crystal Fe/MgO/Fe magnetic tunnel junctions*, Nature Mater. **3** (2004) 868 –871, DOI: 10.1038/nmat1257.

[90] S. Yuasa et al., *High Tunnel Magnetoresistance at Room Temperature in Fully Epitaxial Fe/MgO/Fe Tunnel Junctions due to Coherent Spin-Polarized Tunneling*, J. J. Appl. Phys. **43** (2004) L588–L590, DOI: 10.1143/JJAP.43.L588.

[91] S. Zhang and Z. Li, *Roles of Nonequilibrium Conduction Electrons on the Magnetization Dynamics of Ferromagnets*, Phys. Rev. Lett. **93** (2004) 127204, DOI: 10.1103/PhysRevLett.93.127204.